https://doi.org/10.5194/egusphere-2026-2952
Preprint. Discussion started: 5 June 2026

Ensemble-based global fire modeling as a tool to characterize extreme wildfire events

Andreia F. S. Ribeiro[1], Maik Billing[2], Kirsten Thonicke[2], Werner von Bloh[2], Jakob Wessel[3], Sabine Undorf[2], Matthias Forkel[4], and Jakob Zscheischler[1,4]

[1]Department of Compound Environmental Risks, Helmholtz Centre for Environmental Research—UFZ, Leipzig, Germany
[2]Potsdam Institute for Climate Impact Research, Telegrafenberg A 31, 14473 Potsdam, Germany
[3]Department of Mathematics and Statistics, University of Exeter, Exeter, UK
[4]TUD Dresden University of Technology, Dresden, Germany

Correspondence: Andreia F. S. Ribeiro (andreia.ribeiro@ufz.de)

Abstract. Understanding the full range of possible extreme wildfire events is crucial for risk assessment and adaptation planning. While the historical record offers only one realization of climate, large ensemble simulations sample a broader range of physically plausible climate trajectories, enabling the assessment of rare but realistic extreme events beyond what the observational record alone can reveal. Here we drive the process-based dynamic vegetation-fire model LPJmL-SPITFIRE at the global scale with different climate inputs to produce three sets of simulations: a 40 member large ensemble (40 members × 36 years sample), a single member drawn from the same ensemble (36 years sample), and a reanalysis-driven simulation (36 years sample), with the latter two each representing only a single trajectory of the climate system. This design enables direct comparison of how these two single realizations (single member and reanalysis) versus large ensemble simulations sample the most extreme fire events. We demonstrate that the single realizations are not suited to study risks associated with the most extreme events in fire danger, burned area, and fire carbon emissions that would be possible under current climate conditions. As expected, the highest values in these runs are typically much lower than those of the large ensemble in most regions. The undersampling of extremes by single realizations is greater for fire impacts (burned area and carbon emissions) than for fire danger, highlighting that vegetation–fire feedbacks interact nonlinearly with internal climate variability. While large ensembles reveal more extreme possible events than those simulated with reanalysis and a single climate model ensemble member, they also enable a more robust analysis of the relationship between extreme fire danger and extreme impacts. In particular, the most extreme burned area and emissions do not always coincide with the most extreme fire danger, underscoring the role of non-climatic factors such as ignitions and fuels. Specifically, years with global maximum impacts may occur in years with global fire danger 4.6% - 8.4% lower than the maximum. The findings demonstrate that modeling a broader range of physically plausible wildfire events through large ensemble simulations can help identify the mechanisms leading to the most extreme and high-impact events.

https://doi.org/10.5194/egusphere-2026-2952
Preprint. Discussion started: 5 June 2026

1 Introduction

The need to adapt to unprecedented wildfire outbreaks that are difficult to predict is becoming a reality worldwide, as global warming increases extreme wildfire behavior (Jones et al., 2022, 2024; Cunningham et al., 2025; Kelley et al., 2025). Wildfire activity is known to be driven by multiple climate factors, mainly drought, high temperatures, and low humidity, which can compound in complex ways and are exacerbated with climate change (Ribeiro et al., 2022; Feng et al., 2025; Richardson et al., 2025). In addition to its susceptibility to fire weather, the occurrence of fire also depends on land-use; fuel availability, type and moisture; and ignition sources (natural and anthropogenic) (Forkel et al., 2019; Teckentrup et al., 2019). These drivers and socio-environmental responses are subject to change in a changing climate and society (Jones et al., 2022; Hantson et al., 2024), altering fire regimes in ways that are difficult to anticipate. Methods that can explore a wide range of possible fire extremes beyond what has been observed are hence important (Kelder et al., 2025).

The climate system is inherently stochastic with variability ranging between a number of different time scales: from daily weather variability to monthly or seasonal variability, or long-frequency variability on the order of years to decades that can be driven by, e.g., quasi-periodic ocean circulation patterns (Meyn et al., 2010; Deser et al., 2012). This means that the observed climate is only one realization of the many trajectories that could have occurred, and many studies have emphasized the importance of assessing internal climate variability when analyzing observed or possible changes (Deser et al., 2012; Lehner et al., 2020; Jain et al., 2023). Large ensemble climate model simulations, also known as single-model initial-condition large ensembles (SMILEs), address this by sampling multiple possible realizations of the climate system under the same forcing. Thus, by introducing stochasticity they allow for the assessment of different simulated outcomes and sampling of rare events, including unseen extremes (Kelder et al., 2022; Bevacqua et al., 2023).

To model the climate impact on fire regimes and the subsequent effects on ecosystem functioning and carbon cycling, global fire models have been developed and coupled to Dynamic Global Vegetation Models (DGVMs), which are able to represent the effects of fire disturbances on vegetation as well as feedback mechanisms (Hantson et al., 2020; Oberhagemann et al., 2025). Despite considerable advances in global fire modeling, current modeling approaches often rely on a single realization of climate conditions to drive DGVMs, whether from reanalysis or a single climate model run, each representing only one possible weather trajectory out of the many that could have occurred under the same climate (Hantson et al., 2020; Oberhagemann et al., 2025). Although SMILEs have been previously used to drive impact models (large ensemble climate-impact modeling) this has been limited to simple hydrological and crop models so far (Van Der Wiel et al., 2020; Tschumi et al., 2022, 2023; Lehner, 2024). In contrast, forcing fire-enabled DGVMs with SMILEs has remained a challenge for many reasons. The number of climate input variables required by DGVMs compared to other impact models is larger, resulting in substantial computational costs when forcing complex process-based models with SMILEs. Furthermore, bias-adjustment of climate input is essential for driving DGVMs, and the complexity of bias-adjustment procedures and methodological decisions increases proportionally with the number of variables and size of the large ensemble. Critically, conventional bias-adjustment methods adjusting each ensemble member individually to a single observational reference fail to preserve the primary advantage of using SMILEs in impact modeling: the ensemble spread. To address these challenges, we bias-adjust and downscale a SMILE preserving

https://doi.org/10.5194/egusphere-2026-2952
Preprint. Discussion started: 5 June 2026

modeled internal variability to serve as input to impact models, allowing the exploration of a wide range of possible climates and impacts (Undorf, 2023).

To better understand potential extreme wildfires under present-day climate conditions, here we use the SPread and InTensity of FIRE (SPITFIRE) model (Thonicke et al., 2010; Drüke et al., 2019; Oberhagemann et al., 2025) coupled with the Lund-Potsdam-Jena managed Land (LPJmL, version 5.7.10) DGVM (Schaphoff et al., 2018; Wirth et al., 2024) and forced with the bias-adjusted and downscaled SMILE ACCESS-ESM1-5 (40 members) to generate process-based large ensemble fire simulations. While SPITFIRE has been coupled with other DGVMs besides LPJmL for a number of different applications, including the Fire Model Intercomparison Project (FireMIP, part of the Inter-Sectoral Impact Model Intercomparison Project ISIMIP), these implementations have been driven by reanalysis data or single members from climate model outputs rather than climate large ensembles. Moreover, to date, most of the wildfire research integrating SMILEs has focused on fire weather only (Touma et al., 2021; Quilcaille et al., 2023) or the use of empirical fire models (Keeping et al., 2025). While such studies provide valuable insights into climate-fire weather relationships, they do not fully represent the complex feedback mechanisms between fire disturbance and vegetation dynamics. This study is the first to combine SPITFIRE with large ensemble climate forcing for process-based fire simulation, allowing to sample wildfire events in the tails of the distribution more robustly.

In this work we present a novel use of LPJmL-SPITFIRE via large ensemble climate impact modeling, using reanalysis and bias-adjusted and downscaled climate data from a SMILE as climate inputs. We use this framework to compare output fire simulations across three parallel set-ups: a large ensemble (1440 years sample), a single member (36 years sample) drawn from the ensemble and reanalysis-driven simulation (36 years sample). We address two critical questions: (1) to what extent do large ensembles capture more extreme fire danger, burned area, and carbon emissions than single realizations (a single member drawn from the ensemble and reanalysis); and (2) how the most extreme fire danger (driver) relate to most extreme impacts (burned area and fire carbon emissions). By exploring the full envelope of internal climate variability, this study provides new insights into the range of possible extreme wildfires and the weather conditions that drive them.

2 Methods

In this study, LPJmL-SPITFIRE was forced with different climate inputs to enable the comparison between a large ensemble and individual climate realizations on sampling fire extremes (Figure 1):

1) ACCESS-ESM1-5 SMILE: 40 members climate model large ensemble, bias-adjusted (ensemble spread preserving) and statistically downscaled (section 2.1) between 1979-2014 (40 members × 36 years = 1440 years).

2) Single SMILE member: one member drawn from the ACCESS-ESM1-5 SMILE (r1i1p1f1), representative of standard climate impact assessment frameworks with a single climate model trajectory (including, for example, FireMIP/ISIMIP).

3) Reanalysis: representing the reference climate trajectory during 1979–2014 (i.e., the best estimate of weather conditions that actually occurred in the real world) which corresponds to one realization of the possibly observed climate.

This design allows to quantify the degree to which standard single climate realizations (one member drawn from the SMILE and reanalysis), due to internal climate variability, undersample plausible extremes represented by the large ensemble. To

https://doi.org/10.5194/egusphere-2026-2952
Preprint. Discussion started: 5 June 2026

distinguish between the input forcing (SMILE, single SMILE member and reanalysis) and its corresponding LPJmL-SPITFIRE output, we hereafter refer to the outputs as SMILE-fire, single-fire and reanalysis-fire, respectively (Figure 1).

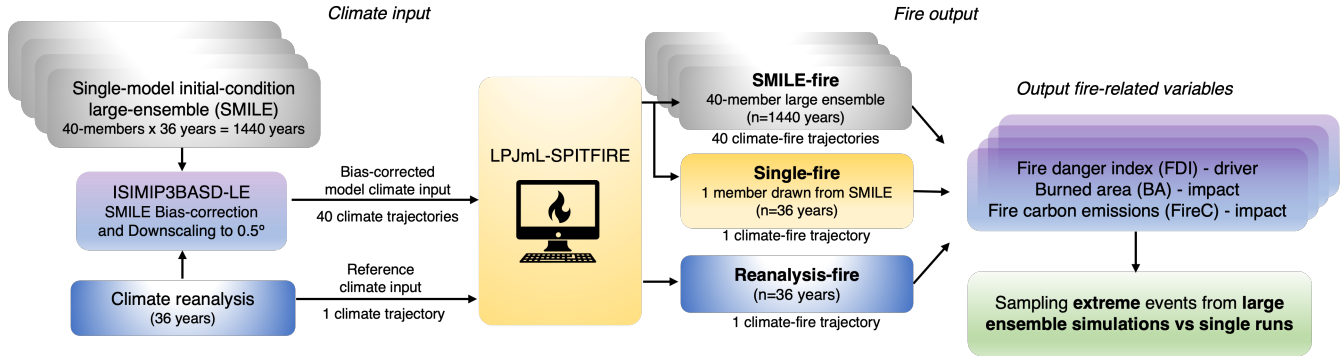

Figure 1. Schematic overview of the modelling workflow used in this study. The climate domain (left) shows the different climate forcing datasets: a single-model initial-condition large-ensemble (SMILE; ACCESS-ESM1-5, 40 members) and the GSWP3-W5E5 climate reanalysis, both covering 1979–2014. SMILE climate data were bias-adjusted and statistically downscaled to a 0.5° × 0.5° global grid using ISIMIP3BASD-LE to preserve internal climate variability across ensemble members (section 2.1). The fire-vegetation domain (right) shows the process-based dynamic global vegetation-fire model LPJmL-SPITFIRE, which was forced with the different climate inputs to produce 3 sets of fire simulations: the full large ensemble labeled 'SMILE-fire' (n = 1440 years), a single ensemble member drawn from the SMILE (r1i1p1f1, n = 36 years) labeled 'single-fire', and a reanalysis-driven simulation (n = 36 years) labeled 'reanalysis-fire'. From the three simulations we analyze the same set of output variables: fire danger index (FDI), burned area (BA), and fire carbon emissions (FireC). These outputs form the basis to compare the range of fire extremes captured by the large ensemble (SMILE-fire) against those from single realizations (single-fire and reanalysis-fire) and characterize ensemble-based extreme relationships between climate drivers (FDI) and fire impacts (BA and FireC). Arrows indicate consecutive research steps and flow of data.

2.1 Bias-adjusting and downscaling large ensemble climate input with ISIMIP3BASD-LE

We used a modified version of the ISIMIP3BASD (Lange, 2019, 2021) bias adjustment and downscaling method tailored to SMILE climate model data, the ISIMIP3BASD-LE (Undorf, 2023) method, to bias-adjust the ACCESS-ESM1-5 (40 members) (Mackallah et al., 2022) SMILE against the GSWP3-W5E5 reference dataset (Dirmeyer et al., 2006; Kim, 2017; Cucchi et al., 2020; Lange et al., 2021). The ISIMIP3BASD-LE method applies the core ISIMIP3BASD bias adjustment (after trend removal and scaling) to the pooled 40 member ensemble, allowing to preserve the modeled internal climate variability in the process. Following ISIMIP3BASD protocol (Lange, 2019, 2020), the bias adjustment is applied at 1.0° spatial resolution globally, for which conservative remapping was used first to remap the ACCESS-ESM1-5 (1.875° × 1.25°) and GSWP3-W5E5 (0.5° × 0.5°) original resolutions to a common 1° × 1° grid. The key daily climate variables required for LPJmL-SPITFIRE forcing were bias-adjusted: longwave and shortwave downward radiation (rlds and rsds), specific humidity (huss), air temperature (tas), maximum and minimum tas (tasmax and tasmin, derived from tas, tasskew and tasrange), precipitation (pr), and near surface wind speed (sfcWind). For training and application periods, the data is split between odd and even years, meaning

https://doi.org/10.5194/egusphere-2026-2952
Preprint. Discussion started: 5 June 2026

that the adjustment is estimated on odd years and applied to even and vice-versa. After bias adjustment the SMILE data is statistically downscaled to 0.5° spatial resolution following the ISIMIP3BASD protocol. Unlike conventional bias-adjustment methods that adjust each member individually, ISIMIP3BASD-LE is designed to adjust marginal distributions preserving the ensemble spread (Figures A1 and A2), a measure of internal climate variability, as discussed in Appendix A. All processing steps, namely climate input bias adjustment, statistical downscaling, and LPJmL-SPITFIRE simulations were performed for 1979-2014, the common period with complete data across all 40 SMILE members and for all required input climate variables. Additional details on the ISIMIP3BASD-LE implementation are provided in Appendix A.

2.2 Forcing LPJmL-SPITFIRE with different climate inputs

We used the LPJmL-SPITFIRE model forced with the bias-adjusted and downscaled SMILE, a single ensemble member drawn from the SMILE, and reanalysis to produce comparable simulations of fire-related variables, hereafter referred to as SMILE-fire, single-fire, and reanalysis-fire, respectively (Fig. 1). Unlike empirical models, which derive statistical relationships between climatic drivers (so-called fire weather) and fire outcomes (e.g. burned area), LPJmL-SPITFIRE explicitly simulates wildfire ignitions, spread and effects on vegetation, along with ecological processes and vegetation feedbacks underlying fire. This means that fire interacts dynamically with vegetation carbon pools, fuel loads, and land surface properties, resulting in mechanistic representation of fire at the global scale (Oberhagemann et al., 2025).

A standard model run consists of two subsequent spin-ups, which bring the model into equilibrium with the climate and land-use forcing, followed by the transient simulation. The first spinup was performed for 3500 years with constant CO_2 (284.73 ppm) and land-use, while the second spinup was performed for 399 years with transient CO_2 (Le Quéré et al., 2015) and land use (Fader et al., 2010). For both spinups the first 30 years of the climatic input (1979-2008) were randomly shuffled and used. After the two spinups, the model ran in transient mode for 36 years using reanalysis climate data from 1979-2014. For the human and natural ignition component of SPITFIRE, the transient run used population density (Klein Goldewijk et al., 2011) and lightning flashes from the OTD/LIS satellite product (Christian et al., 2003). For more technical information about LPJmL-SPITFIRE, we refer the reader to Oberhagemann et al. (2025) and Appendix B.

In contrast to the simulations forced with the reanalysis GSWP3-W5E5 (reanalysis-fire), which uses a single deterministic climate forcing, the large ensemble simulations include 40 different climate input datasets (40 members × 36 years = 1440 years). To ensure identical initial conditions of the transient run across the different ensemble members, both spin-up phases were performed using climate forcing from a single ensemble member (r1i1p1f1). As the spin-up serves only to bring the model to equilibrium, we expect the choice of concrete ensemble member to play a minor role. All LPJmL-SPITFIRE transient ensemble simulations were then initialized from the same restart file. We tested the sensitivity of this approach by performing the second spin-up (399 years) separately for each SMILE member, and the difference in the ensemble spread was negligible (not shown).

https://doi.org/10.5194/egusphere-2026-2952
Preprint. Discussion started: 5 June 2026

2.3 Analysis of LPJmL-SPITFIRE model output in terms of fire-related variables

Based on the generated simulations (SMILE-fire, single-fire and reanalysis-fire) we analyzed three LPJmL-SPITFIRE output fire-related variables: fire danger index (FDI) based on the vapor pressure deficit (VPD) (Drüke et al., 2019), burned area (BA) and fire carbon emissions (FireC). To compare LPJmL-SPITFIRE fire outputs with reference fire records, the 5th version of the Global Fire Emissions Database (GFEDv5.1) (Chen et al., 2023; Van Der Werf et al., 2017; van der Werf et al., 2025) was used for burned area and fire carbon emissions. The GFEDv5.1 products were aggregated from their original 0.25° spatial resolution to 0.5° (cdo gridboxsum). Both datasets include small fires at the monthly scale. Because LPJmL-SPITFIRE restricts the simulation of wildfires occurring to natural vegetation, we excluded croplands, peatlands, and deforestation fires from GFEDv5.1.

We analyzed the LPJmL-SPITFIRE fire-related output variables (FDI, BA and FireC) at both global and regional scales, with all analyses performed on annual values. The BA and FireC were summed over each calendar year and the annual maximum FDI was calculated. Area-weighted mean values were calculated for FDI, while BA and FireC were spatially aggregated at global and regional scales by summing grid cell values globally and across the 14 GFED regions (Giglio et al., 2006) (Figure C1) for both GFEDv5.1 and LPJmL-SPITFIRE simulations. Given that the LPJmL-SPITFIRE does not reproduce the observed human-induced declining trend in burned area (Andela et al., 2017; Oberhagemann et al., 2025) all data were linearly detrended to enable comparisons independent of trends (Figure C2). Seasonal patterns are not analyzed due to LPJmL-SPITFIRE limitations in representing fire behavior in areas where fire spread occurs at the end of the year (Figure C3), arising from temporal resolution mismatches between the vegetation and fire components (Oberhagemann et al., 2025).

2.3.1 Comparing large ensembles with single realizations

For each detrended fire-related variable (FDI, BA and FireC) at the annual time-scale and GFED region, we compared the pooled large ensemble SMILE-fire (40 members × 36 years = 1440 years) against the single-fire (36 years) and reanalysis-fire (36 years) simulations. By construction, pooling the 40 members (1440 years) allows the SMILE-fire to sample considerably rarer events than any single 36 years simulation. The single realizations are therefore expected to systematically undersample the most extreme events. To quantify this, we computed for each detrended fire-related variable X the relative difference between the maxima values of each single realization and the pooled SMILE-fire simulations as

$$\Delta_{\max} = \frac{\max(X_{single}) - \max(X_{SMILE-fire})}{\max(X_{SMILE-fire})} \times 100 \quad (1)$$

where $\max(X_{single})$ corresponds to the single realization (single-fire or reanalysis-fire) largest annual value (anomalies of annual maximum FDI, anomalies of annual total BA, or anomalies of annual total FireC) over 1979-2014 (36 years sample). The $\max(X_{SMILE-fire})$ corresponds to the maximum annual value of the pooled 40-member SMILE-fire (1440 years sample). Positive values indicate that single realizations maximum value exceeds the SMILE-fire maximum value, while negative values indicate undersampling of rarer events by single realizations. Additionally, we computed the 95th (p95), 97.5th (p97.5), and 99th (p99) percentile thresholds of the SMILE-fire, corresponding to progressively rarer events within

https://doi.org/10.5194/egusphere-2026-2952
Preprint. Discussion started: 5 June 2026

the 1440-years sample. In terms of return periods, these thresholds correspond to approximately 1-in-20 years (p95), 1-in-40 years (p97.5), and 1-in-100 years (p99), computed as 1/(1-p) applied to the pooled sample. Of these, p97.5 is the closest to the expected return period of the maximum value from the 36-year single realizations (1-in-36 years).

2.3.2 Ensemble-based extreme driver-impact relationships

We used the SMILE-fire simulations to assess the relationship between extreme FDI (driver) and extreme fire impacts (BA and FireC). For each ensemble member, we consider the maximum value of FDI, BA and FireC at annual resolution (i.e., the maximum of the full 36-year period for each variable and ensemble member). We then conditionally sampled extremes by extracting FDI values corresponding to the year in which BA or FireC attain their maximum over the full period, and vice versa. For a single realization, this yields one maximum value over the 36-year period. In contrast, the SMILE-fire large ensemble provides 40 such values (one per ensemble member), enabling a more robust characterization of conditional and unconditional distributions of extremes. Specifically, for each SMILE-fire ensemble member, we extract extreme values of FDI, BA and FireC for two conditions. The first impact-focused condition corresponds to the FDI (driver) at maximum BA ($FDI|BA_{max}$) or FireC ($FDI|FireC_{max}$). This condition describes whether extreme impacts require extreme drivers. The second driver-focused condition corresponds to the impact (BA or FireC) at maximum FDI ($BA|FDI_{max}$ or $FireC|FDI_{max}$). This condition shows whether extreme drivers always produce extreme impacts.

We compare the SMILE-fire conditional and unconditional distributions (FDI_{max}, BA_{max}, and $FireC_{max}$) to assess the coupling between drivers (FDI) and impacts (BA and FireC) within the large ensemble SMILE-fire. Similar ensemble climate-impact approaches have been used to identify compounding climate drivers of extreme impacts (Bevacqua et al., 2021, 2023; Zscheischler et al., 2014; Van Der Wiel et al., 2020; Lehner, 2024). To assess the extent to which extreme fire danger drives extreme fire impacts, we calculated:

$$\Delta_{\text{cond}} = \frac{\min(\mathrm{X}_{cond}) - \min(\mathrm{X}_{uncond})}{\min(\mathrm{X}_{uncond})} \times 100 \quad (2)$$

where X_{cond} represents 40 conditional samples (e.g., $FDI|BA_{max}$) and X_{uncond} represents 40 unconditional samples (e.g., FDI_{max}). For example, $\Delta_{FDI|BA_{max}}$ compares the minimum value of the 40 FDI values when BA was at its maximum (across members) to the minimum FDI_{max}. Since FDI_{max} is by definition the maximum FDI over all 36 years of a single member, it is always greater or equal to the conditional FDI. Therefore, $\Delta_{\text{cond}} \leq 0$ by construction. While values near zero indicate that extremes in both variables tend to co-occur, negative values indicate that FDI_{max} does not necessarily coincide with BA_{max} and $FireC_{max}$. This was calculated both globally and separately for each of the 14 GFED regions.

3 Results

3.1 Interannual spread and general patterns of wildfire simulations

At both global and regional scales (GFED regions), the single realizations (single-fire and reanalysis-fire) lie within the absolute spread of the SMILE-fire (Figures 2 and C4). In particular, the interquartile ranges are very similar at both global

https://doi.org/10.5194/egusphere-2026-2952
Preprint. Discussion started: 5 June 2026

and regional scales among the LPJmL-SPITFIRE simulations, indicating consistent variability in fire behavior (Figures 2 and C5). Nevertheless, the SMILE-fire simulates a broader range of extreme values than captured by either the reanalysis-fire or single-fire simulation due to the wider representation of the internal climate variability by the large ensemble (Figures 2 and C4). When pooling all ensemble members, the SMILE-fire extremes are consistently larger than those in single simulations at global, regional and pixel-level scales (Figures 2 boxplots, C4, C6, C7 and C8).

The strength of the pairwise linear relationships between the fire-related annual variables at the global scale is generally comparable across the different LPJmL-SPITFIRE simulations (Figure 2d,e,f). Nevertheless, the SMILE-fire's larger sample size (1440 years sample) enables a more robust characterization of extreme events compared to the single-fire and reanalysis-fire simulations. The strongest relationship is between BA vs FireC (impacts, Figure 2f), followed by FDI (driver) vs FireC (Figure 2e) and FDI vs BA (Figure 2d). This hierarchy of correlations aligns with the process-based structure in LPJmL-SPITFIRE, where fire danger influences fire occurrence probability but does not fully determine fire spread (BA) and carbon emissions. The tight coupling between BA vs FireC is expected as fire emissions are calculated from burned area and fire intensity, which itself is a function of burned area in LPJmL-SPITFIRE (Figure B1). The more modest correlations between FDI (driver) and fire impacts (BA and FireC) reflect the additional factors required for fire occurrence as ignitions and fire spread/fire size, leading to higher variability.

We compare with the GFEDv5.1 in the common period of 2002-2014. The LPJmL-SPITFIRE simulations show good agreement with GFEDv5.1 in terms of global interannual variability (Figure 2a–c). In terms of pairwise relationships, GFEDv5.1 has lower correlation between global BA and FireC compared to the LPJmL-SPITFIRE simulations, which can however be an artifact of the short common time period (Figure 2f). Despite an overall good spatial agreement between LPJmL-SPITFIRE and GFEDv5.1, regional and pixel-level comparisons suggest discrepancies in northern Australia and equatorial Asia (EQAS) for both BA and FireC (Figures C4–C7), consistent with Oberhagemann et al. (2025). In terms of spatial variability, northern hemisphere South America (NHSA) and equatorial Asia (EQAS) exhibit the highest interquartile ranges in FDI (Figure C5), while southern hemisphere South America (SHSA), northern hemisphere Africa (NHAF), and southern hemisphere Africa (SHAF) show greater variability in fire impacts (BA and FireC) according to LPJmL-SPITFIRE (Figure C4 and C5).

3.2 Large ensemble fire simulations allow sampling of very extreme events

Single realizations systematically undersample the SMILE-fire most extreme value of the three fire-related variables in the majority of GFED regions, with both single-fire and reanalysis-fire simulations showing negative Δ_{max} in most of the regions (Figures 3 and 4). For FDI, both the single-fire and reanalysis-fire simulations show negative Δ_{max} in all regions, confirming consistent undersampling of extreme fire danger by single realizations in contrast to SMILE-fire (Figures 3a and 4a). The largest differences occur in EURO (-59.3% single-fire Figure 3a, -73.5% reanalysis-fire Figure 4a) and TENA (-39.9% single-fire, -62.7% reanalysis-fire), while MIDE (-18.5% single-fire, -19.7% reanalysis-fire) and BONA (-36.2% single-fire, -35.1% reanalysis-fire) show relatively smaller but still undersampling. This uniform negative Δ_{max} suggests that neither single simulation type captures the full range of possible fire danger extremes that would be possible in the current climate, regardless of region.

https://doi.org/10.5194/egusphere-2026-2952
Preprint. Discussion started: 5 June 2026

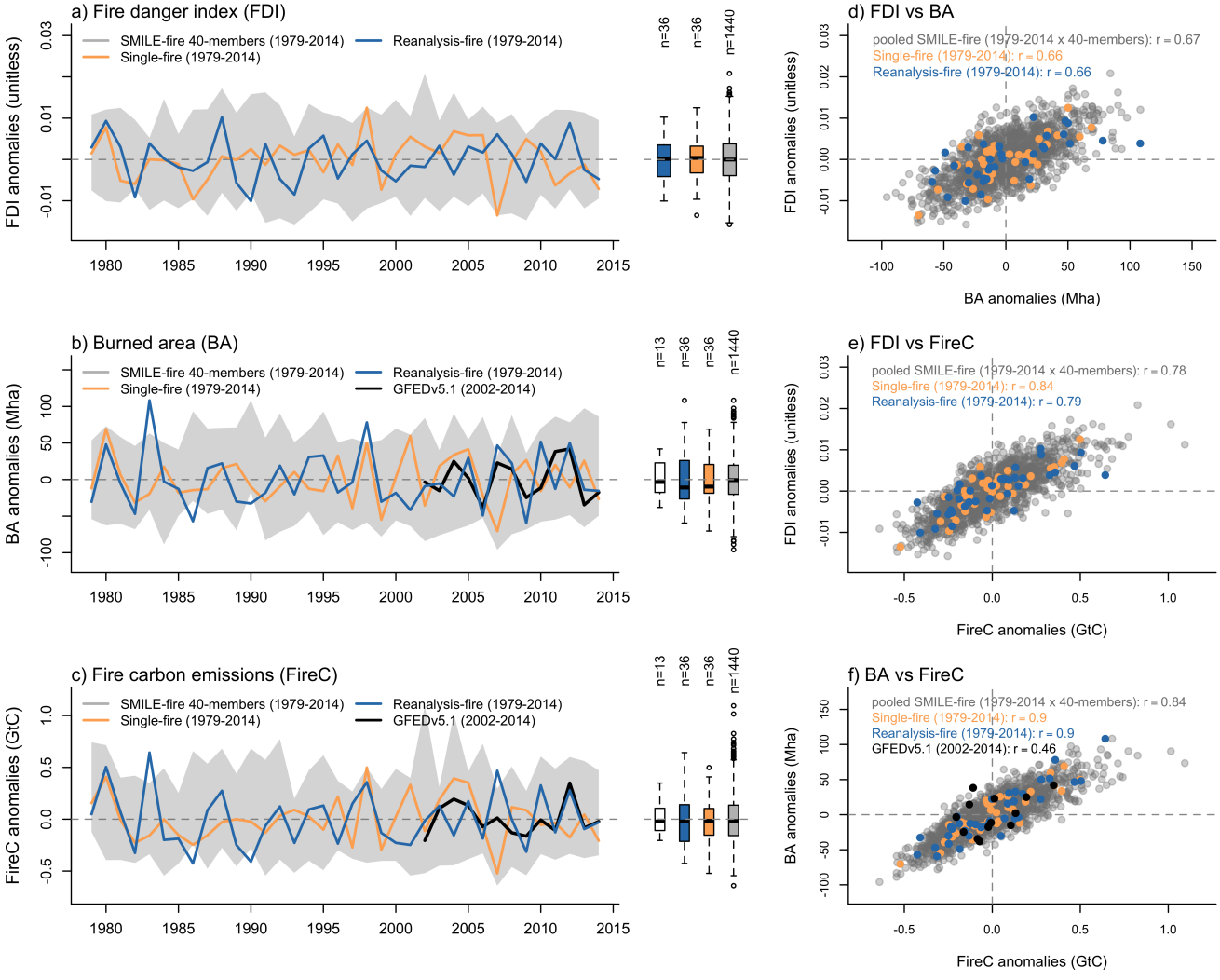

Figure 2. Global fire-related variables simulated by LPJmL-SPITFIRE (1979–2014) and from the Global Fire Emissions Database version 5.1 (GFEDv5.1; 2002–2014) for reference. Time-series panels show (a) global weighted-average annual maximum fire danger index (FDI), (b) global annual total burned area (BA), and (c) global annual total fire carbon emissions (FireC). Four datasets are shown: the 40-member large ensemble labeled 'SMILE-fire' (gray shading, full ensemble range), a single ensemble member labeled 'smile-fire' (yellow), a reanalysis-fire simulation labeled 'reanalysis-fire' (blue), and GFEDv5.1 reference data (black in time series and scatter plots; white in boxplots). Boxplot whiskers extend to 1.5 times the interquartile range from the 25th and 75th percentiles. Scatter plots show pairwise relationships between FDI and BA (d), FDI and FireC (e), and BA and FireC (f), with the linear correlation r reported for each dataset. All data were linearly detrended over the periods shown to enable trend-independent comparisons.

https://doi.org/10.5194/egusphere-2026-2952
Preprint. Discussion started: 5 June 2026

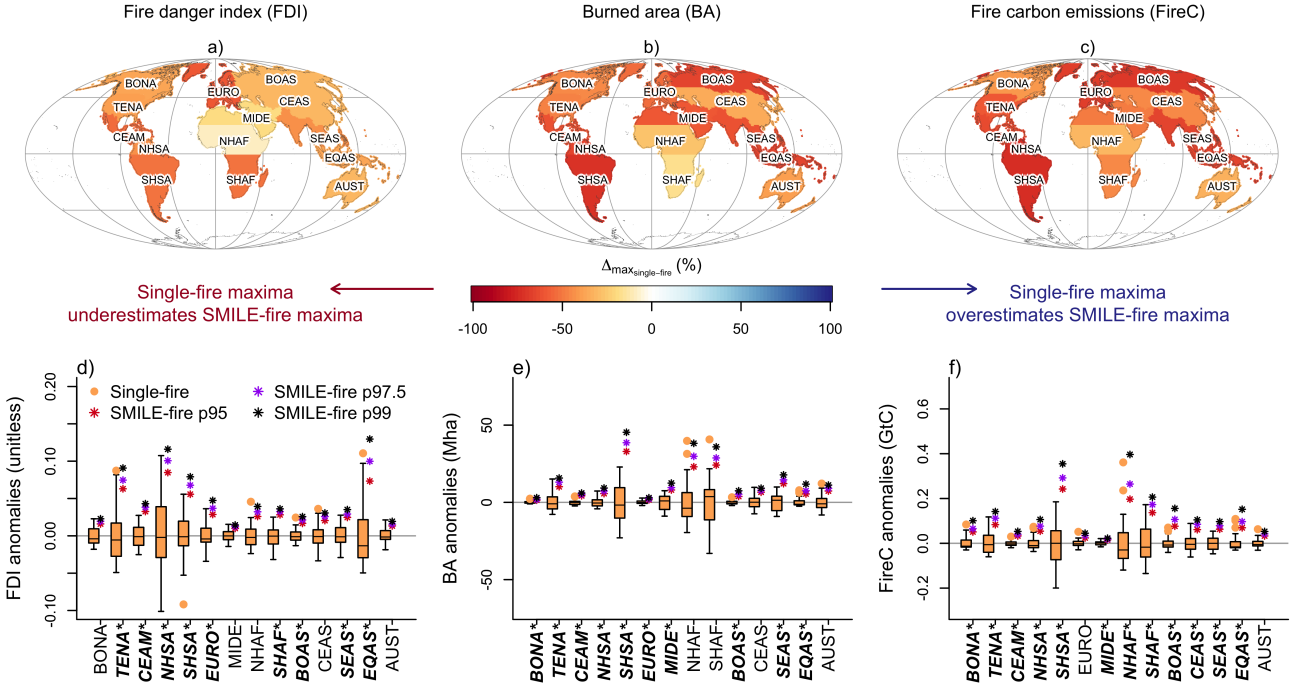

Figure 3. Percentage relative difference between LPJmL-SPITFIRE single-fire simulation (36 years) and 40-member large ensemble (SMILE-fire, 1440 years) maxima across GFED fire regions. Global maps (a–c) show Δ_{max} (Eq. 1) for (a) fire danger index (FDI), (b) burned area (BA), and (c) fire carbon emissions (FireC). Negative values (red, orange, and yellow) indicate that the single-fire maximum falls below the SMILE-fire maximum, suggesting undersampling of extremes; positive values (blue) indicate overestimation. The 14 regions follow the GFED classification: BONA (Boreal North America), TENA (Temperate North America), CEAM (Central America), NHSA (Northern Hemisphere South America), SHSA (Southern Hemisphere South America), EURO (Europe), MIDE (Middle East), NHAF (Northern Hemisphere Africa), SHAF (Southern Hemisphere Africa), BOAS (Boreal Asia), CEAS (Central Asia), SEAS (Southeast Asia), EQAS (Equatorial Asia), and AUST (Australia). Regional boxplots (d–f) show the distribution of single-fire simulations (36 years) alongside the 95th (red), 97.5th (purple), and 99th (black) percentile thresholds of the SMILE-fire, computed by pooling all 40 ensemble members (1440 years). Regions where the SMILE-fire 99th percentile exceeds the single-fire maximum are marked with bold italic labels and an asterisk (*) on the x-axis. All variables were linearly detrended.

In terms of BA and FireC impacts, the single-fire simulation consistently underestimates extremes across both variables and regions, as expected from a single 36-year sample (Figure 3b,c). The reanalysis-fire simulation also generally undersamples BA and FireC extremes, with the exception of Boreal North America (BONA), Central America (CEAM), and Northern Hemisphere Africa (NHAF) (Figure 4b,c). Despite the few exceptions, the FireC reanalysis-fire simulation shows the greater undersampling in EURO (-88.1%), BOAS (-84.2%), and TENA (-79.8%). In general, the magnitude of undersampling by both

https://doi.org/10.5194/egusphere-2026-2952
Preprint. Discussion started: 5 June 2026

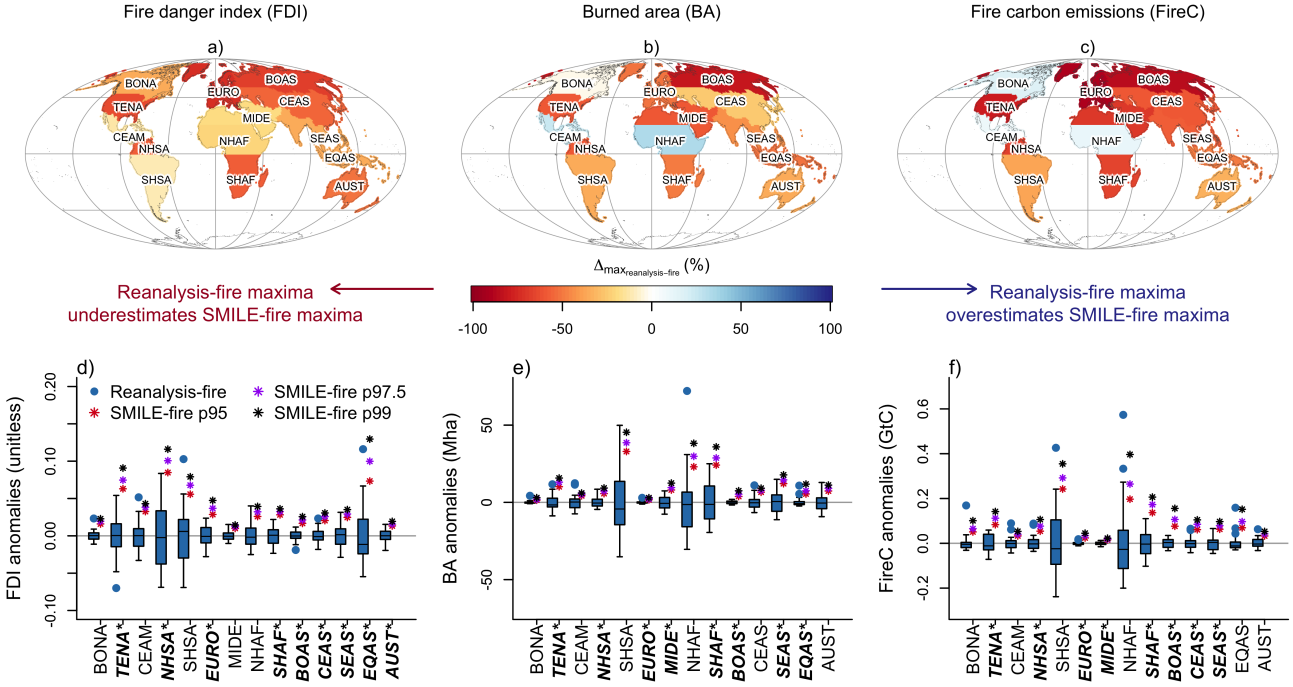

Figure 4. Same as Figure 4 but for the reanalysis-fire LPJmL-SPITFIRE simulation rather than the single-fire simulation.

single simulations is generally larger for fire impacts (BA and FireC) than for the FDI (climate driver). While the BA single-member simulation exhibits the strongest undersampling in SHSA (-70.1%), the BA reanalysis-fire strongest undersampling occurs in BOAS (-80.2%). In terms of FireC, the single-member simulation largest Δ_{max} occurs in SHSA (-72.2%).

As a sensitivity analysis, Figures 3d-f and Figures 4d-f display the respective full range of the single realizations in contrast with progressively rarer extreme percentiles of the pooled SMILE-fire (95th, 97.5th and 99th, respectively p95, p97.5 and p99). For FDI, the SMILE-fire simulation p99 exceeds the maximum range of both the single-fire and reanalysis-fire simulations in 9 out of the 14 GFED regions (Figure 3d and 4d), indicating undersampling of 1-in-100 year events by the single realizations in these areas. Despite the fact that a sample of 36 years cannot be expected to regularly capture a 1-in-100-year event, the results demonstrate that SMILE-fire provides unique value in characterizing the most extreme events in contrast to single realizations. Even for 1-in-40-year events (p97.5), which are closer in frequency to the most extreme events expected in a 36-year single realization, the SMILE-fire ensemble exceeds the upper whisker of the boxplot (defined as 1.5 × interquartile range above the 75th percentile) in several regions (despite not always surpassing the highest individual outlier). This indicates that the SMILE-fire captures more frequent and intense extreme values than empirically possible in the shorter simulations.

https://doi.org/10.5194/egusphere-2026-2952
Preprint. Discussion started: 5 June 2026

3.3 Relationships between extreme fire danger and impacts

We now examine each SMILE-fire member individually to unfold relationships between drivers (FDI) and impacts (BA and FireC) within individual climate trajectories. The distribution of the pooled SMILE-fire FDI (driver) is illustrated in Figures 5a and 6a. Based on the 40 members, the SMILE-fire BA_{max} (impact, Figure 5b) and SMILE-fire $FireC_{max}$ (impact, Figure 6b) from each member are identified in the SMILE-fire FDI distribution (blue vertical tick marks in Figures 5a and 6a). This corresponds to the impact-focused conditional sampling of FDI ($FDI|BA_{max}$ and $FDI|FireC_{max}$), which we compare against the unconditional sampling FDI_{max} for each ensemble member (yellow shading region in Figures 5a and 6a) to illustrate whether extreme impacts require extreme drivers. The spread of the SMILE-fire FDI conditional sampling tends to be larger than the SMILE-fire FDI unconditional sampling, with longer lower tails. In other words, a few ensemble members achieve maxima impacts (BA_{max} and $FireC_{max}$) in years without maximum fire danger (impact-focused condition) (Figures 5 and 6a,b). This means that the SMILE-fire enables us to explore extreme impact wildfires under a range of possible non-extreme fire danger, that would be missed by using a single simulation with its limited sampling. Specifically, when FDI is conditioned on BA_{max} ($FireC_{max}$) (Figures 5 and 6a,b), years with BA_{max} ($FireC_{max}$) can experience FDI conditions that are -4.6% (-8.4%) below the lowest FDI_{max} across the 40 ensemble members (Δ_{cond} in Eq. 2).

In the same fashion, the SMILE-fire FDI_{max} (driver, Figure 5a and Figure 6a) for each member are identified in the impact distributions of SMILE-fire BA and FireC (yellow vertical tick marks in Figures 5b and 6b). Similarly, the FDI_{max} of a few ensemble members do not translate into the largest impacts. Specifically, years with FDI_{max} may yield to BA (FireC) values -14.1% (-16.2%) below the lowest BA_{max} ($FireC_{max}$). This means that FDI_{max} is not a sufficient condition for extreme impacts. The joint distributions of driver vs impacts include $FDI|BA_{max}$ vs $BA|FDI_{max}$ and $FDI|FireC_{max}$ vs $FireC|FDI_{max}$ and confirm that many extreme impacts occur under non-extreme fire danger (blue dots in 5c and 6c), and many extreme FDI events do not lead to extreme burned area (yellow dots in 5c and 6c). This decoupling reflects the influence of non-climatic factors modulating fire activity rather than fire danger alone.

The values of Δ_{cond} vary considerably across the 14 GFED regions (Figures 5e and 6e), ranging from near zero in some regions (suggesting co-occurrence of extreme FDI and impacts) to highly negative values in others. For $FDI|BA_{max}$, the Δ_{cond} can go up to -26.9% in EURO, indicating that factors like fuel structure or ignitions may enable large fires even without peak fire weather. Similarly, Δ_{cond} $BA|FDI_{max}$ shows larger values up to -54.9% in EURO, meaning that even at peak fire danger, burned area reaches less than half of its potential maximum in EURO. For $FDI|FireC_{max}$, the Δ_{cond} goes up to -20.0% in CEAS and NHSA, indicating that extreme carbon emissions can occur under sub-maximal FDI. Similarly, Δ_{cond} $FireC|FDI_{max}$ shows much larger negative values up to -55.6% in BOAS, meaning that even at peak fire danger, emissions often reach less than half of their FireC potential maximum in BOAS.

In general, the discordance is more evident when impacts (BA and FireC) are conditioned on FDI maxima rather than when FDI is conditioned on maxima impacts. Across the SMILE-fire ensemble, more individual members simulate peak FDI without coinciding maximum impacts, while fewer members simulate peak impacts without peak fire danger (tick marks in Figures 5a,b and 6a,b). This reveals that peak FDI is a necessary but not sufficient driver of extreme fire impacts: while BA_{max} and

https://doi.org/10.5194/egusphere-2026-2952
Preprint. Discussion started: 5 June 2026

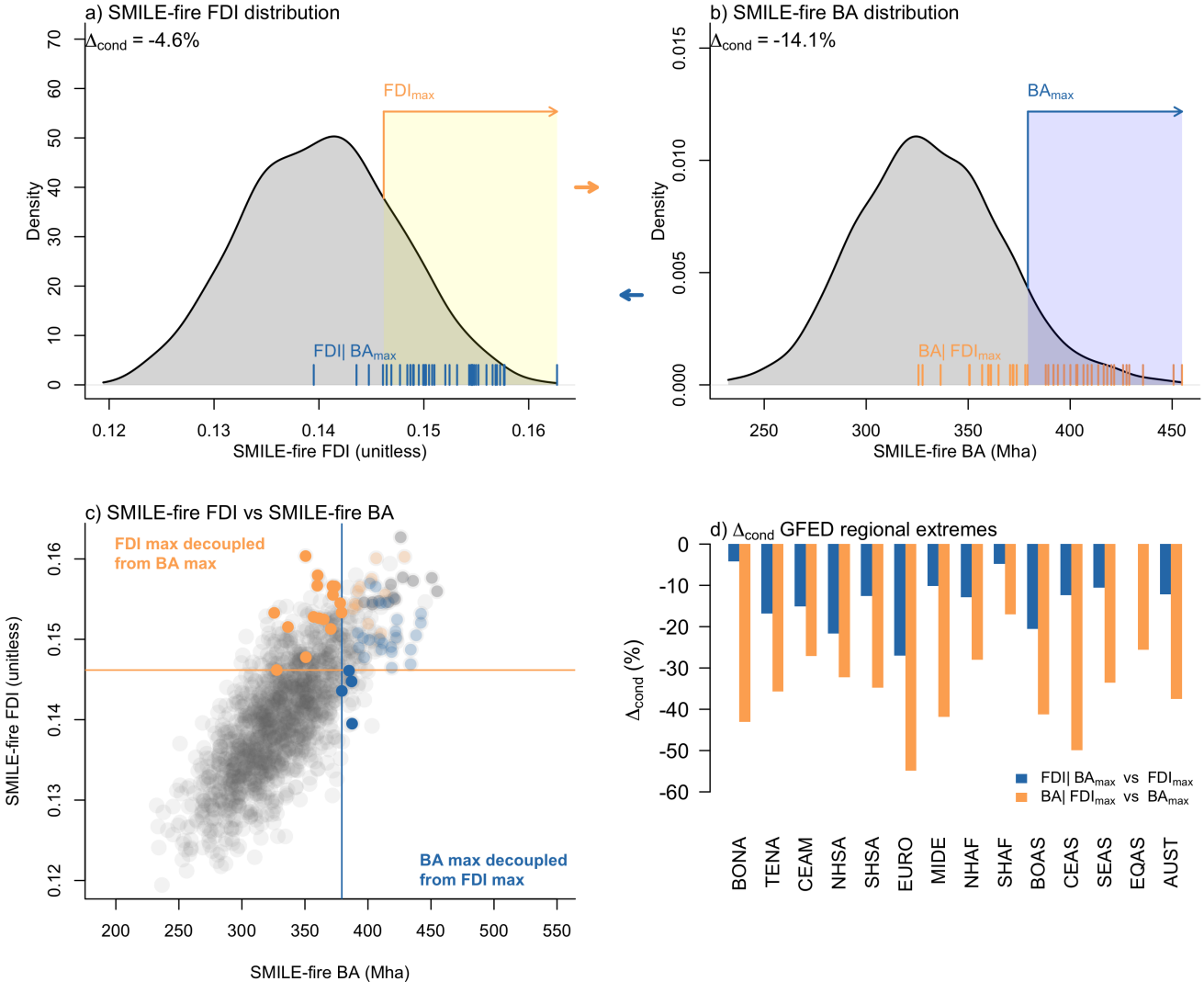

Figure 5. Relationship between fire danger index (FDI) and burned area (BA) maxima across SMILE-fire at global and regional scales. Probability densities of global FDI (a) and BA (b) pooling all 40 ensemble members (gray). (a) Yellow shading marks values above the lowest FDI_{max} across each member (40 unconditional values), and blue vertical tick marks indicate $FDI|BA_{max}$ (40 conditional values). (b) Blue shading marks values above the lowest BA_{max} (40 unconditional values), and yellow vertical tick marks indicate $BA|FDI_{max}$ (40 conditional values). (a,b) Top left global Δ_{cond} defined as the relative difference between the conditional and unconditional minima (Eq. 2). (c) The joint distribution of global FDI and BA across all ensemble members and years: gray dots represent all years; yellow filled dots indicate years when FDI reaches its member maximum but BA does not; blue filled dots indicate years when BA reaches its member maximum but FDI does not; transparent yellow and blue dots indicate years when both variables simultaneously reach their member maximum. Vertical lines mark the minimum unconditional thresholds for FDI (yellow) and BA (blue). (d) Regional Δ_{cond} values for each of the 14 GFED regions. Panels a) and b) were inspired by Figure 3 of Van Der Wiel et al. (2020).

https://doi.org/10.5194/egusphere-2026-2952
Preprint. Discussion started: 5 June 2026

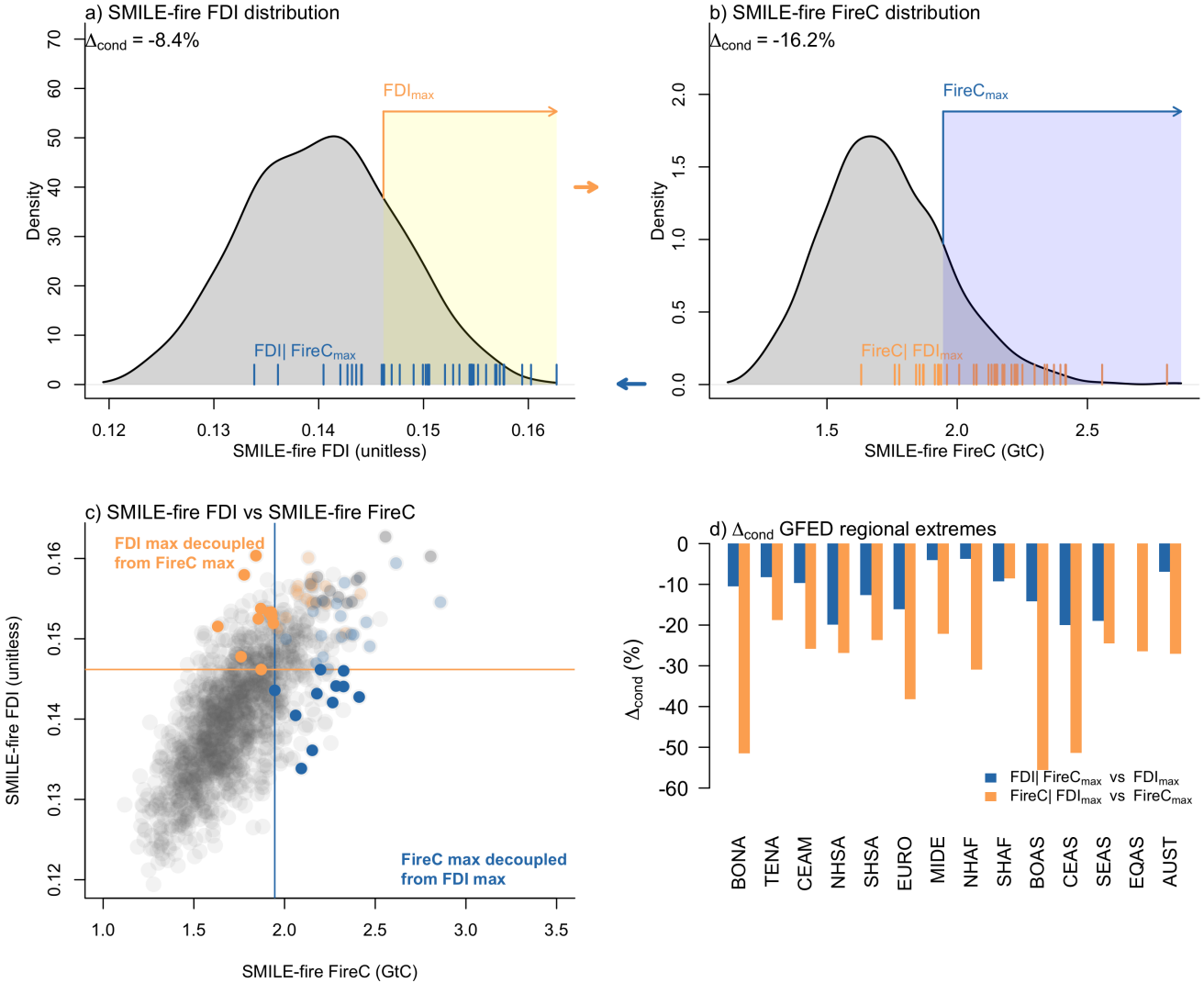

Figure 6. Same as Figure 5 for fire carbon emissions.

https://doi.org/10.5194/egusphere-2026-2952
Preprint. Discussion started: 5 June 2026

$FireC_{max}$ may occur without the FDI_{max}, it is more possible that FDI_{max} occurs without producing BA_{max} or FDI_{max}. Similarly to Figures 3 and 4 where EURO and BOAS were among the regions where single realizations undersample extremes the most, these are also regions with more discordance between conditional and unconditional maxima, highlighting the critical role of other factors rather than climate conditions conducive of fire extremes. These findings underscore the critical role of ecosystem processes in modulating fire outcomes, which are explicitly captured in LPJmL-SPITFIRE. While fire weather only studies lack the mechanistic representation of vegetation–fire feedbacks needed to explain why extreme fire danger does not always lead to extreme impacts, relying on a single realization, even with a process-based model, underestimates extremes due to insufficient sampling of internal climate variability. By combining a fire-enabled DGVM with a large ensemble, both the broad range of climate variability and the underlying ecosystem controls on fire can be robustly represented.

4 Discussion and conclusions

This study demonstrates that single climate realizations undersample physically plausible fire extremes captured by large ensemble simulations, particularly the more extreme values. Due to internal climate variability we can expect extremes beyond those captured by single realizations to occur, presenting a critical challenge for fire risk assessment. This applies not only to simulations conducted with climate reanalysis but also to the simulations driven by a single climate model run, as commonly done in state-of-the-art climate impact assessment frameworks (Warszawski et al., 2014). Our analysis reveals that neither single realization fully captures the broader range of fire extremes that would be possible under the current climate, and that very extreme fires are possible under moderately extreme fire danger levels. This suggests that storylines (Shepherd et al., 2018; Sillmann et al., 2021) leading to the most extreme fires should be explored in more detail, in particular the combinations of compounding favorable fire weather with high fuel availability, fuel moisture, and ignition patterns, that single realizations do not sample comprehensively (Zscheischler et al., 2020; Bevacqua et al., 2023).

The SMILE-fire simulations are particularly valuable for studying fire impact variables, burned area and fire carbon emissions, compared to the climate driver, fire danger. For most regions, the maxima of single realizations rank below those of SMILE-fire, with fire carbon emissions from single realizations showing the largest undersampling. In other words, smaller changes in fire danger extremes due to internal variability have the potential to trigger stronger responses in burned area and emissions. This can be explained by nonlinearities and vegetation-fire feedbacks. While fire danger tends to respond more linearly to changes in climate forcing, the transition from fire driver to actual fire outcomes involves threshold behaviors and vegetation-fire feedbacks that can push ecosystems past critical states, triggering a larger response in fire outcomes than fire danger. Moreover, fire carbon emissions are particularly more sensitive because they depend not only on burned area but also on fuel load and combustion completeness, and thus exhibit higher sensitivity to the role of internal climate variability on the process-based modeling chain.

The potential for extremes beyond those captured by reanalysis and a single member drawn from SMILE-fire varies markedly by region. At the regional scale, the SMILE-fire captures higher maxima of fire-related variables than both the reanalysis and single-member in nearly all GFED regions, except for boreal north America (BONA), central America (CEAM) and northern hemisphere Africa (NHAF). These exceptions, though modest, may be related with factors relevant for the stochasticity of

https://doi.org/10.5194/egusphere-2026-2952
Preprint. Discussion started: 5 June 2026

fires in boreal and tropical regimes that are not incorporated in our large ensemble scheme. For example, it could be the case that for the same probability of lightning (which is not different across ensemble members in our case), any of the SMILE members synchronizes the rare combinations of fire danger and fuels captured by the reanalysis. In some cases, the single-member simulations might also include the most extreme event of the SMILE by chance. Although a finite number of ensemble members cannot fully encompass all physically possible climate-fire interactions, the ensemble of 40 members used here sample a substantially broader range of climate trajectories than single realizations, consistently revealing stronger impacts across most regions.

There are some limitations of the present study to note. The LPJmL-SPITFIRE fire danger is based on VPD with plant functional types (PFT)-specific tuning parameters and the live fuel moisture levels are calculated based on a growing season index (Oberhagemann et al., 2025). While VPD captures the atmospheric demand for moisture, it does not directly incorporate other meteorological variables that more comprehensive fire danger indices such as the Canadian Fire Weather Index (FWI) (Wagner, 1987) which includes wind and precipitation. While wind speed drives fire spread in the Rothermel model (see Appendix B for LPJmL-SPITFIRE model structure) and precipitation acts on vegetation state and fire behavior through process-based components, neither is explicitly captured in the FDI itself. Thus, while LPJmL-SPITFIRE framework does account for meteorological variables beyond VPD, their contributions are not explicit in what we refer here is as 'climate driver', as we define it through FDI (VPD-based). Disentangling the relative roles of other climate drivers beyond FDI constitutes an important avenue for future work. Particularly, assessing the ensemble-based relationships between climate drivers and extreme impacts (burned area and carbon emissions) could be generalized to a broader set of climate variables beyond FDI, including wind speed, precipitation, and large-scale atmospheric circulation patterns. Such an approach would allow exploring physically self-consistent combinations of drivers governing extreme fires, in line with physical climate storyline methods. This framework can equally be extended on the impact side to the full range of LPJmL-SPITFIRE outputs, namely fire size, fire duration, number of fires, and vegetation mortality, enabling a more comprehensive characterization of extreme fire events beyond the burned area and fire carbon emissions examined here.

Beyond hydrometeorological drivers, topography and fire ignition assumptions are aspects that future work could further address. Satellite-derived lightning products have inherently limitations (Christian et al., 2003) and human-caused ignition based on population density (Thonicke et al., 2010) does not fully capture human ignition behavior driven by, for example, land management practices or socioeconomic factors (Ribeiro et al., 2024; Forrest et al., 2024). Furthermore, lightning ignition probability is held constant across ensemble members, and thus does not respond to changes in convective activity associated with different climate states. As a result, while fire weather favorable conditions across the ensemble members amplify the fire outcomes of the same prescribed ignitions, lightning cannot itself act as a source of climate-driven variability in the simulations. Future work could include climate model output of lightning-related variables to allow ignition probability to respond dynamically to the climate state, enabling a more complete representation of natural climate variability in fire activity (Janssen et al., 2023).

It should be noted that while LPJmL-SPITFIRE produces reasonable estimates of mean burned area and fire carbon emissions, its performance in modeling extreme fires remains less explored. In particular, SPITFIRE represents surface fire spread but does

https://doi.org/10.5194/egusphere-2026-2952
Preprint. Discussion started: 5 June 2026

not explicitly simulate crown fire or canopy fire spread, which are characteristic of the most extreme fire events in boreal and other fire-prone ecosystems (Ward et al., 2018). Additionally, including the influence of wind and precipitation on live fuel moisture computation would furter contribute to improve extreme fire danger conditions and to separate the influence of wind speed on fire spread from the influence of atmospheric drying of the fuel. Beyond process representation, the observational benchmarks used to validate LPJmL-SPITFIRE (Oberhagemann et al., 2025) are typically drawn from GFED databases, and cross-comparison against additional products (e.g. Table 7 in Li et al. (2026)) would provide a more robust assessment of model performance, particularly in the extremes where observational uncertainty is largest. The choice of calibration dataset directly influences model behavior in the extremes, hence model development, calibration and benchmarking using different observational fire products could therefore yield meaningfully different representations of extreme fire events. In this sense, the large ensemble framework is itself a tool for understanding model behavior in the extremes: due to increased sample size, large ensembles deliberately sample the extremes that the model can produce, making the performance in that range visible and open to evaluation in future work.

While climate models and vegetation-fire process-based models are powerful tools to understand climate-vegetation-fire relationships, they are computationally expensive at the global scale using large ensembles. For this reason, frameworks such as ISIMIP rely on single realizations across multiple climate models and process-based models, missing an adequate representation of the response to climate variability. However, these selected models typically underestimate uncertainties related to internal climate variability and varying model structure in key sectors at the global scale (Bevacqua et al., 2026). While our analysis consists of one SMILE paired with one impact model, a single SMILE already provides multiple realizations of internal variability as represented by one climate model. Combining multiple SMILEs with multiple process-based vegetation-fire models would further enable explicit separation of the contribution of internal variability from structural model uncertainty (Lehner, 2024). Extended to future fire projections, a key area of study for the fire modeling community with high societal relevance (Keeping et al., 2025; Quilcaille et al., 2023), would additionally need to account for varying socio-economic scenarios (Lehner, 2024), which can be highly relevant for fire ignition and suppression. This remains computationally and methodologically challenging. While these barriers are important to overcome for concrete wildfire risk and impact quantification, the illustrated added value of using large ensemble climate data holds nonetheless.

A key methodological consideration in this work is that the offline modeling approach used here (driving LPJmL-SPITFIRE with a SMILE) requires bias adjustment and statistical downscaling of the climate input variables. In particular, the ISIMIP3BASD-LE procedure aligns the input large ensemble with a single observed climate realization, the reanalysis, constraining the range of attainable values of each climate variable (e.g. 2m temperature) to those present in the reanalysis. However, fire conditions are rarely determined by a single variable in isolation: they emerge from compound combinations of dryness, heat, low humidity, extreme wind, and fuel moisture that co-occur in physically consistent ways. The frequency of such compound combinations is still substantially enlarged by the large ensemble scheme relative to a single realization, and we therefore expect this to constitute a significant added value of the large ensemble framework demonstrated here. Furthermore, the ISIMIP3BASD implementation applied here bias-adjusts the pooled ensemble members rather than each member individually (Lange, 2019), which preserves the variance across different members and avoids artificially constraining the ensemble spread.

https://doi.org/10.5194/egusphere-2026-2952
Preprint. Discussion started: 5 June 2026

The ensemble-impact modelling approach demonstrated here is transferable in method and rationale to other impact sectors beyond wildfires. In agriculture and hydrology, analogous added value of large ensembles has already been documented (van der Wiel et al., 2019; Van Der Wiel et al., 2020; Bevacqua et al., 2021; Vogel et al., 2021; Lehner, 2024), suggesting that the findings identified here reflect a general feature of ensemble climate-impact modeling. Systematic application of large ensemble impact frameworks across socio-ecological sectors would therefore inform society much more comprehensively on climate-related risks, in ways that approaches relying in single realizations cannot support.

Appendix A: The ISIMIP3BASD-LE

A1 Large ensemble bias-adjustment and downscaling

The ISIMIP3BASD-LE (Undorf, 2023) consists of a modified version of the ISIMIP3BASD Lange (2019, 2020). Based on ISIMIP3BASD-LE, the 40 member ACCESS-ESM1-5 model ensemble (Mackallah et al., 2022) was bias-adjusted to correct systematic biases while preserving modelled internal climate variability. In contrast to ISIMIP3BASD, which was designed to process only single realizations (r1i1p1f1), ISIMIP3BASD-LE applies the core steps of the ISIMIP3BASD method (after detrending and scaling which are applied to each ensemble member individually) to a pooled ensemble, thus creating a richer climate model dataset from which bias adjustment transfer functions can be derived. This allows to better preserve the ensemble spread and systematic differences between the ensemble members, compared to adjusting each member individually. The core of the ISIMIP3BASD consists of a trend transfer by quantile to construct 'pseudo-future observations', together with a parametric or nonparametric (depending on the variable and the quality of the parametric fit) quantile mapping, inspired by Switanek et al. (2017). We refer to Lange (2019, 2021) and the changelog in Lange (2020) for more details.

Before applying the bias adjustment both observational data and each ensemble member are remapped to a common 1.0° global resolution grid, using conservative remapping (cdo remap). The bias adjustment is then applied at this resolution, independently to each gridcell. We bias adjust air temperature (tas), precipitation (pr), shortwave and longwave downward radiation (rsds and rlds), wind speed (sfcWind), relative humidity (hurs), surface air pressure (ps), daily temperature range (tasrange = tasmax - tasmin) and daily temperature skew (tasskew = (tas-tasmin)/tasrange). Daily minimum and maximum temperature (tasmin, tasmax) are subsequently obtained from tas, tasrange and tasskew. Out-of-sample application of the method is important as when applied in-sample the observations might be perfectly reconstructed (e.g. Spuler et al., 2024, 2026). Thus we split the data into training and application period by considering odd and even years independently (cmp. Lange, 2019), using the odd years to define the bias adjustment transformation function to adjust the even years and vice-versa. The ISIMIP3BASD-LE method is applied in a running window with a window size of 31 and a step size of 3 days. Whilst this step size is slightly larger than the default of 1 day for ISIMIP3BASD, we found this to be of minor importance and it allowed for substantial computational savings.

Figure A1 shows the empirical cumulative distribution functions (ECDFs) of observations as well as the ECDFs of the SMILE members before and after bias adjustment. The observational ECDFs are captured by the range of bias adjusted model

https://doi.org/10.5194/egusphere-2026-2952
Preprint. Discussion started: 5 June 2026

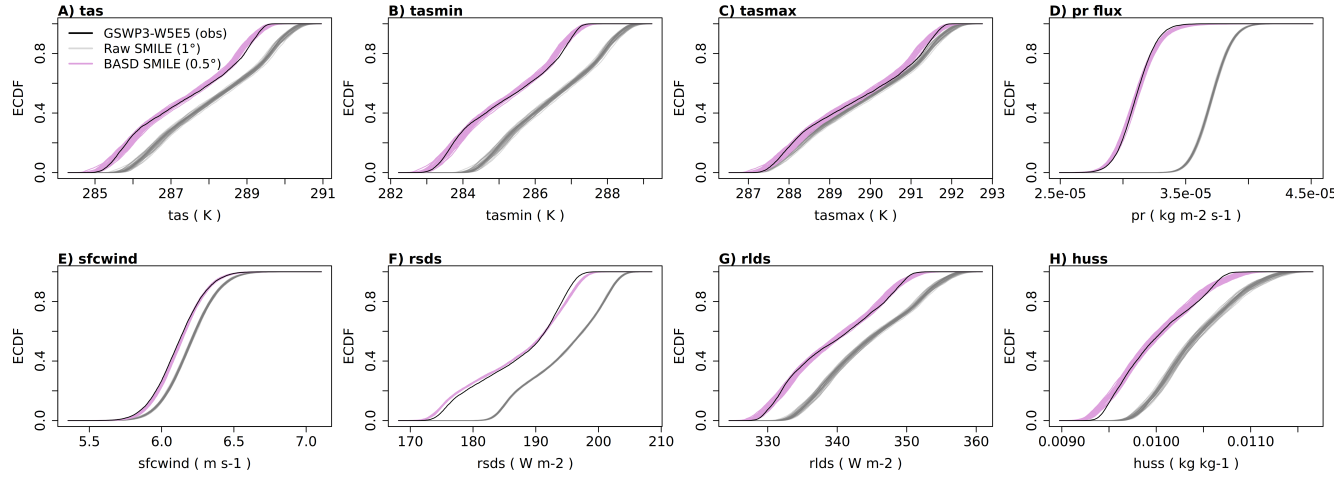

Figure A1. Empirical cumulative distribution functions (ECDFs) of spatially averaged tas (average temperature), tasmax (maxmimum temperature), tasmin (minimum temperature), precipitation (pr), surface wind (sfcwind), surface downwelling longwave and shortwave radiation (rlds and rsds), specific humidity (huss); ACCESS-ESM1-5 before (gray) and after bias-adjustment and downscaling with ISIMIP3BASD-LE (purple).

ECDFs, which suggest successful out-of-sample application on the global scale. Further, some difference between the model ECDFs seems to be preserved, suggesting that structural differences between ensemble members remain.

After bias adjustment and merging of the individually adjusted odd and even years the MBCnSD method, part of ISIMIP3BASD, was used to statistically downscale each ensemble member at 1° × 1° to 0.5° × 0.5° resolution. The MBCnSD method builds upon the MBCn algorithm by Cannon (2018). A key advantage of this method is that it preserves values at the aggregated spatial resolution, meaning the weighted sum of all downscaled time series within one coarse grid cell equals the original coarse-resolution value. This ensures consistency across spatial scales and maintains the statistical properties of the bias adjusted large ensemble.

To quantify the preservation of modelled internal climate variability throughout the bias-adjustment and downscaling procedures, we calculated the ensemble standard deviation (as measure of the ensemble spread) of daily global averages (cdo ensstd). For each day t, the ensemble standard deviation $\sigma(t)$ is given by:

$$\sigma(t) = \sqrt{\frac{1}{M-1}\sum_{m=1}^{M}\left(\overline{X}_m(t) - \overline{X}_M(t)\right)^2} \tag{A1}$$

where $\overline{X}_m(t)$ is the spatially averaged value of variable X for ensemble member m on day t, $\overline{X}_M(t)$ is the ensemble mean across all members on day t, and M is the number of ensemble members. Finally, we averaged $\sigma(t)$ in time and calculated the spread ratio of the bias-adjusted (BASD) data to that in the raw data:

$$\text{Spread Ratio} = \frac{\sigma_{\text{BASD}}}{\sigma_{\text{raw}}} \tag{A2}$$

https://doi.org/10.5194/egusphere-2026-2952
Preprint. Discussion started: 5 June 2026

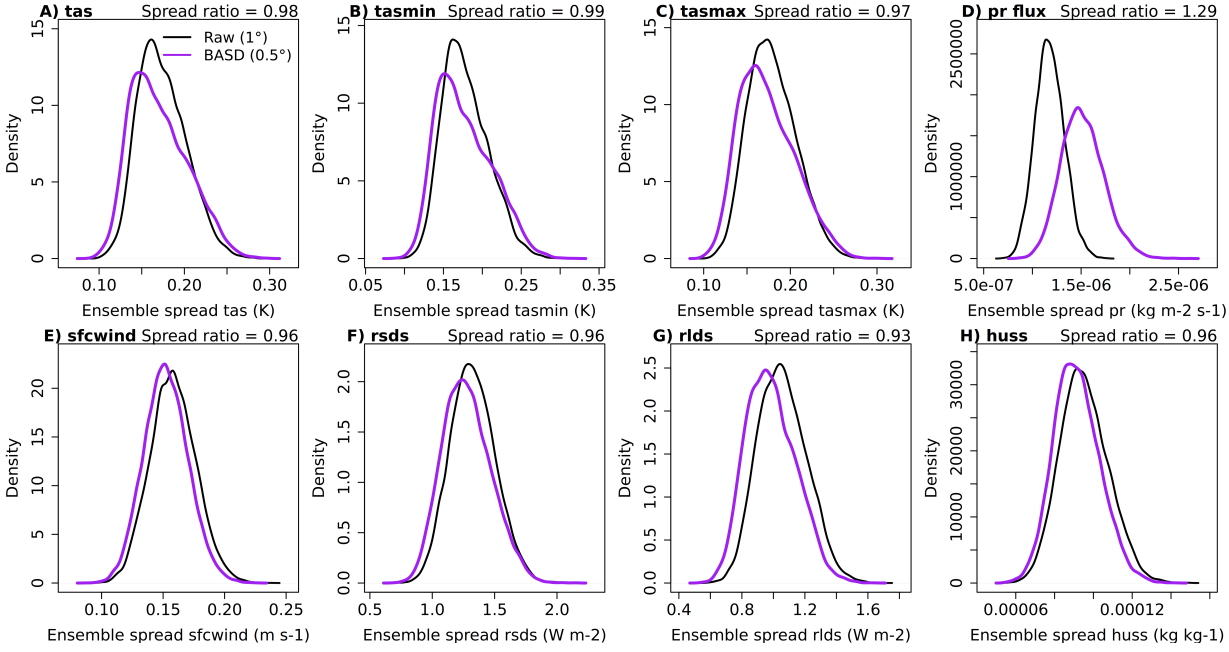

Figure A2. Ensemble standard deviation $\sigma(t)$ (Equation A1) of daily global averages, before (black) and after bias-adjusted and downscaling with ISIMIP3BASD-LE (purple). The top left values indicate the spread ratio defined in Equation A2.

Density plots of Equation A2 are shown in Figure A2. Ensemble spreads seem preserved after bias adjustment and downscaling (values close to 1), meaning that this does not artificially suppress or amplify the range of climate outcomes represented in the large ensemble.

Bias-adjustment and downscaling were performed using Python (ISIMIP3BASD-LE and ISIMIP3BASD), with supporting data operations implemented via Bash, CDO, and NCO. Major computational challenges included I/O bottlenecks, time dimension re-ordering in netCDF files, and attribute management, with operations on concatenated ensemble data cubes proving particularly resource-intensive. For these reasons, the final step of enforcing variable limits (Lange, 2020, 2021) after bias adjustment and statistical downscaling was performed using mathclm which is part of the LPJmL utilities.

Appendix B: The LPJmL-SPITFIRE

B1 Model structure

LPJmL-SPITFIRE is a fire-enabled DGVM that is able to simulate the impact of wildfires on vegetation dynamics, and vice-versa (Oberhagemann et al., 2025). In this modeling framework, vegetation dynamics are simulated by the LPJmL model (Schaphoff et al., 2018; Von Bloh et al., 2018), while SPITFIRE represents the fire module that is coupled to LPJmL . The coupled LPJmL-SPITFIRE model explicitly accounts for the impacts of wildfires on vegetation structure and composition, as

https://doi.org/10.5194/egusphere-2026-2952
Preprint. Discussion started: 5 June 2026

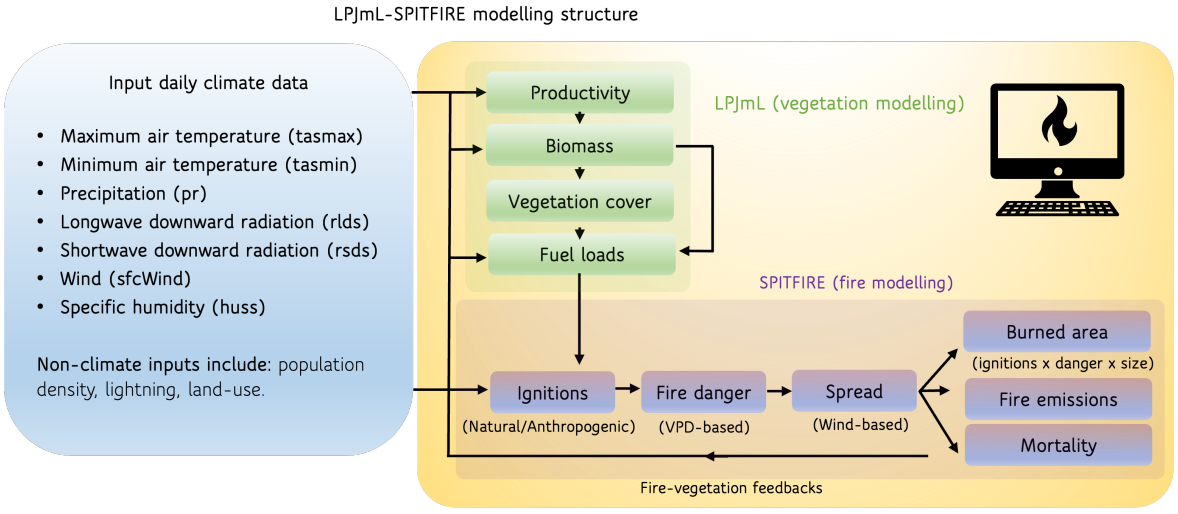

Figure B1. Systems diagram describing model–data integration of LPJmL-SPITFIRE, adapted from Thonicke et al. (2010), Drüke et al. (2019) and Oberhagemann et al. (2025).

well as feedbacks of vegetation properties on fire occurrence, spread, and intensity. SPITFIRE calculates fire disturbance by simulating the fire danger, ignition, spread, and the impacts of fire separately (Oberhagemann et al., 2025). The main features of SPITFIRE (Fig. B1) are published in Thonicke et al. (2010) and recent improvements were included in Drüke et al. (2019) and Oberhagemann et al. (2025). SPITFIRE requires daily climate input of maximum and minimum air temperature, precipitation, longwave and shortwave downward radiation, wind, and humidity. As non-climate input data, population density and lightning flashes are also required. Main SPITFIRE output variables are fire danger, burned area, fire emissions and number of fires (Fig. B1). While previous versions of SPITFIRE used the Nesterov Index (based on maximum temperature, dew point temperature and the different plant functional types) for calculating fire danger, recently Drüke et al. (2019) implemented a VPD-based fire danger. The duration of the fire is determined by the fire danger index and assumes a longer burn time under high fire danger. SPITFIRE considers two types of ignition sources: lightning flashes and human ignitions determined based on population density (see Eqs. 3 and 4 in Thonicke et al. (2010)). The Rothermel equations are employed to determine fire spread, which also varies according to plant functional types. Finally, the model uses the simulated fire danger, ignitions, and spread to estimate burned area and fire carbon emissions. The model restricts the simulation of wildfires occurring to natural vegetation, excluding managed land, such as agriculture, due to fundamentally different fire dynamics in this type of land (Ribeiro et al., 2024).

https://doi.org/10.5194/egusphere-2026-2952
Preprint. Discussion started: 5 June 2026

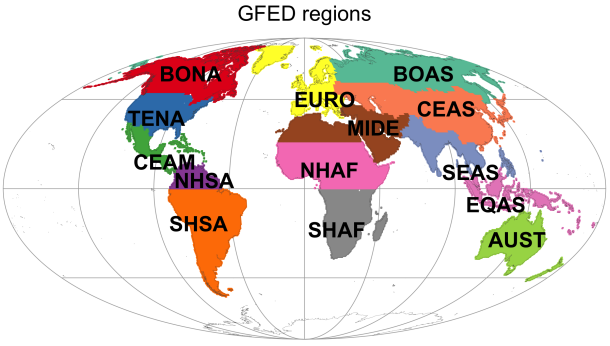

Figure C1. Global Fire Emissions Database (GFED) regions: BONA (Boreal North America), TENA (Temperate North America), CEAM (Central America), NHSA (Northern Hemisphere South America), SHSA (Southern Hemisphere South America), EURO (Europe), MIDE (Middle East), NHAF (Northern Hemisphere Africa), SHAF (Southern Hemisphere Africa), BOAS (Boreal Asia), CEAS (Central Asia), SEAS (Southeast Asia), EQAS (Equatorial Asia), and AUST (Australia).

Appendix C: Additional Figures

. **Code Availability.** The used version of LPJmL-SPITFIRE is archived on Zenodo at https://doi.org/10.5281/zenodo.1473450 by (Oberhagemann et al., 2025). The code for bias-correction is made available by Undorf (2023) in https://zenodo.org/records/10377116 and for downscaling in https://doi.org/10.5281/zenodo.2549631 by Lange (2020).

. **Data Availability.** The GSWP3-W5E5 reanalysis (Dirmeyer et al., 2006; Kim, 2017; Cucchi et al., 2020; Lange et al., 2021) is made available by the ISIMIP3a portal (https://files.isimip.org/ISIMIP3a/InputData/climate/atmosphere/obsclim/global/daily/historical/GSWP3-W5E5/). The ACCESS-ESM1-5 data is made available by the Earth System Grid Federation (ESGF) nodes (https://esgf-metagrid.cloud.dkrz.de/search). The GFEDv5.1 data is made available by van der Werf et al. (2025) (https://zenodo.org/records/16794692). The LPJmL-SPITFIRE large ensemble simulations and reanalysis-driven generated and used in this study are available at https://doi.org/10.5281/zenodo.19709419.

. **Author's contribution.** AFSR conducted the analysis and led the writing of the manuscript. JZ and KT contributed to the design of the overall research. SU and JW provided expertise and guidance on bias-adjustment. MB and WvB contributed technical expertise on LPJmL-SPITFIRE implementation and configuration. MB curated the GFEDv5.1 data. MF, JZ, KT, SU, JW, MB and WvB provided critical feedback at multiple stages. All the authors contributed to the writing of the manuscript.

https://doi.org/10.5194/egusphere-2026-2952
Preprint. Discussion started: 5 June 2026

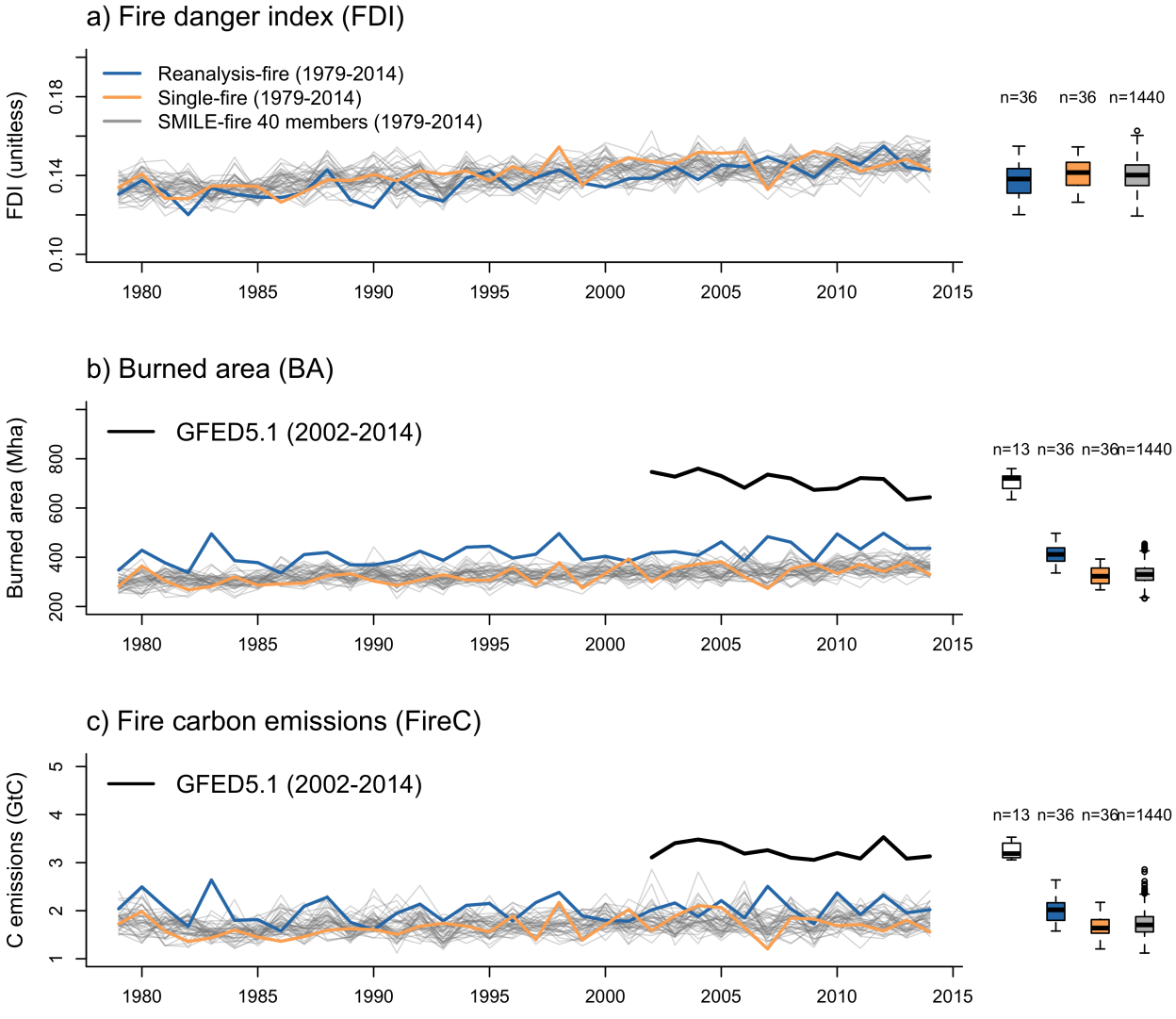

Figure C2. Same as Figure 2 before detrending.

https://doi.org/10.5194/egusphere-2026-2952
Preprint. Discussion started: 5 June 2026

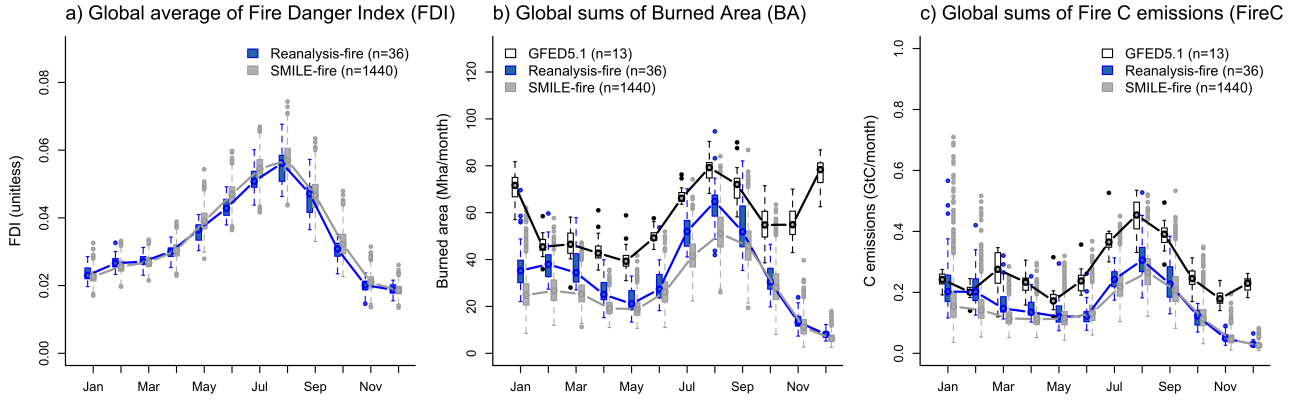

Figure C3. Monthly spread of fire danger index (FDI) (left), fire carbon emissions (center) and burned area (right) of GFEDv5.1 (black, 2002-2014), LPJmL-SPITFIRE (1979-2014) reanalysis (blue) and large ensemble (gray). Data not detrended.

. **Competing interests.** The authors declare that no competing interests are present.

475 . **Acknowledgments.** AFSR acknowledges the Alexander von Humboldt Foundation (AvH) for a postdoctoral fellowship and the Deutsche Forschungsgemeinschaft (DFG) - Project number 530175554. JZ acknowledges the Helmholtz Initiative and Networking Fund (Young Investigator Group COMPOUNDX, Grant Agreement VH-NG-1537). AFSR acknowledges the contributions of Markus Druke and Karin van der Wiel in initial stages of the designing of the study and to Karl Ebert who validated initial simulations with a different version of LPJmL-SPITFIRE as part of an undergrad internship. AFSR also acknowledges the contribution of Sebastian Ostberg in the implementation
480 of the LPJmL version (5.7.10) within the ISIMIP protocol and the EVE team at UFZ for the IT support with the LPJmL installation and configuration.

https://doi.org/10.5194/egusphere-2026-2952
Preprint. Discussion started: 5 June 2026

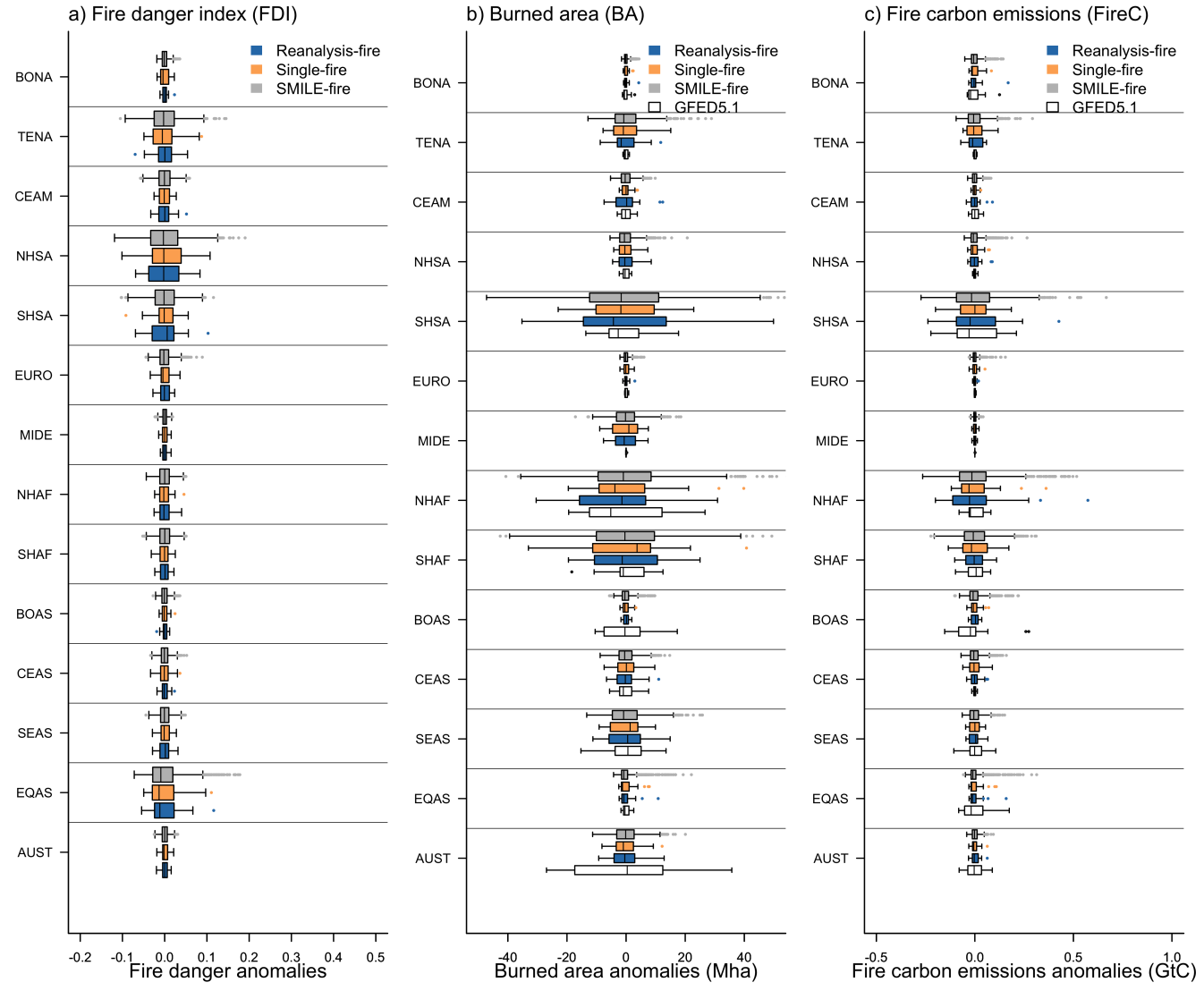

Figure C4. Annual maximum values of fire danger (a), annual fire carbon emissions (b), and annual burned area across 14 GFED regions (c) and different LPJmL-SPITIFRE simulation settings for 1979-2014 (large ensemble - gray, single-member run r1i1p1f1 - yellow, and reanalysis - blue). Remote sensing observations are shown in black and white for comparison (2002-2014). The 14 regions follow the GFED classification: BONA (Boreal North America), TENA (Temperate North America), CEAM (Central America), NHSA (Northern Hemisphere South America), SHSA (Southern Hemisphere South America), EURO (Europe), MIDE (Middle East), NHAF (Northern Hemisphere Africa), SHAF (Southern Hemisphere Africa), BOAS (Boreal Asia), CEAS (Central Asia), SEAS (Southeast Asia), EQAS (Equatorial Asia), and AUST (Australia). All variables are linearly detrended.

https://doi.org/10.5194/egusphere-2026-2952
Preprint. Discussion started: 5 June 2026

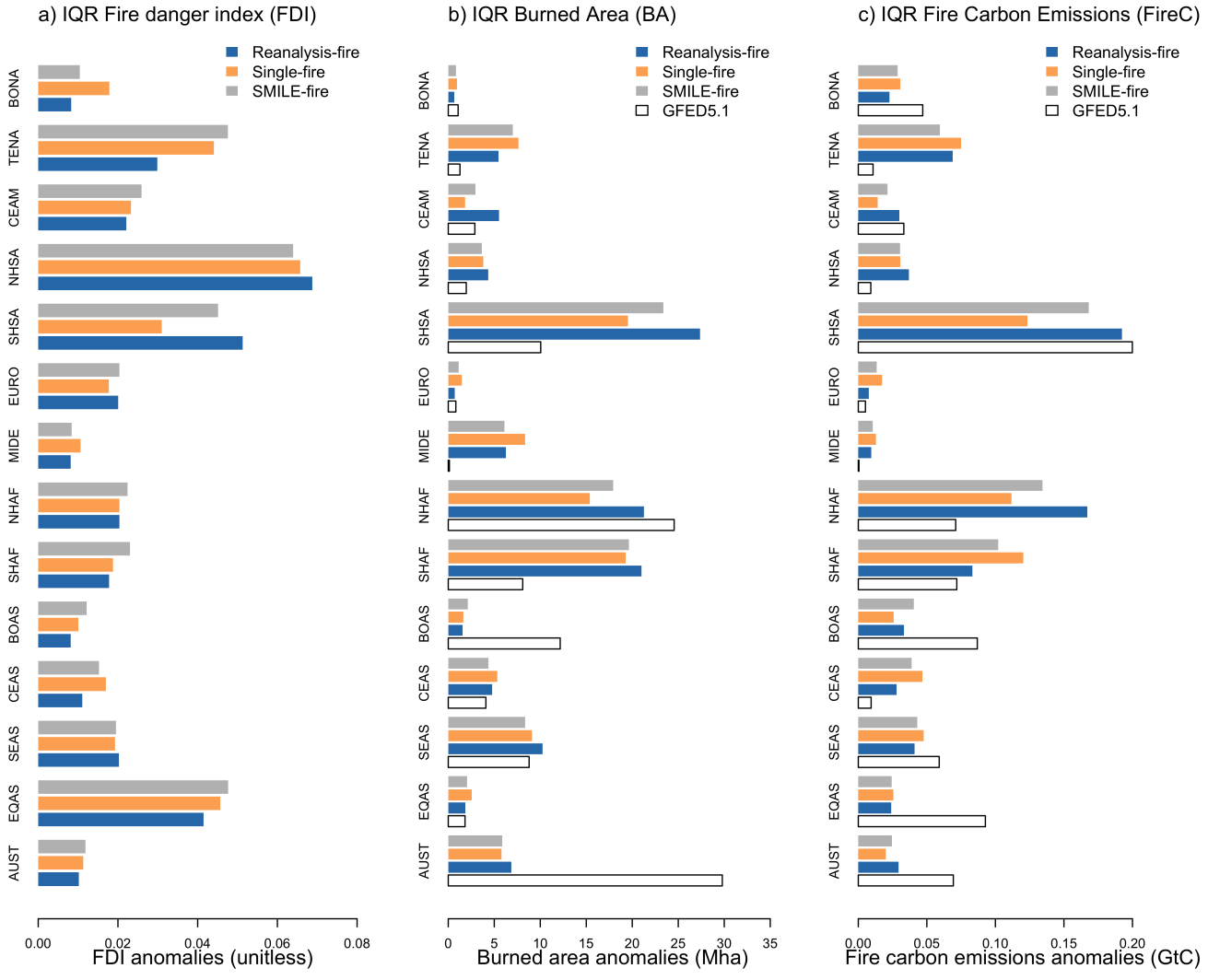

Figure C5. Interquartile range (IQR) of annual maximum values of fire danger (a), annual fire carbon emissions (b), and annual burned area (c) across 14 GFED regions and different LPJmL-SPITIFRE simulation settings for 1979-2014 (large ensemble - gray, single-member run r1i1p1f1 - yellow, and reanalysis - blue). Remote sensing observations are shown in black and white for comparison (2002-2014). The 14 regions follow the GFED classification: BONA (Boreal North America), TENA (Temperate North America), CEAM (Central America), NHSA (Northern Hemisphere South America), SHSA (Southern Hemisphere South America), EURO (Europe), MIDE (Middle East), NHAF (Northern Hemisphere Africa), SHAF (Southern Hemisphere Africa), BOAS (Boreal Asia), CEAS (Central Asia), SEAS (Southeast Asia), EQAS (Equatorial Asia), and AUST (Australia). All variables are linearly detrended.

https://doi.org/10.5194/egusphere-2026-2952
Preprint. Discussion started: 5 June 2026

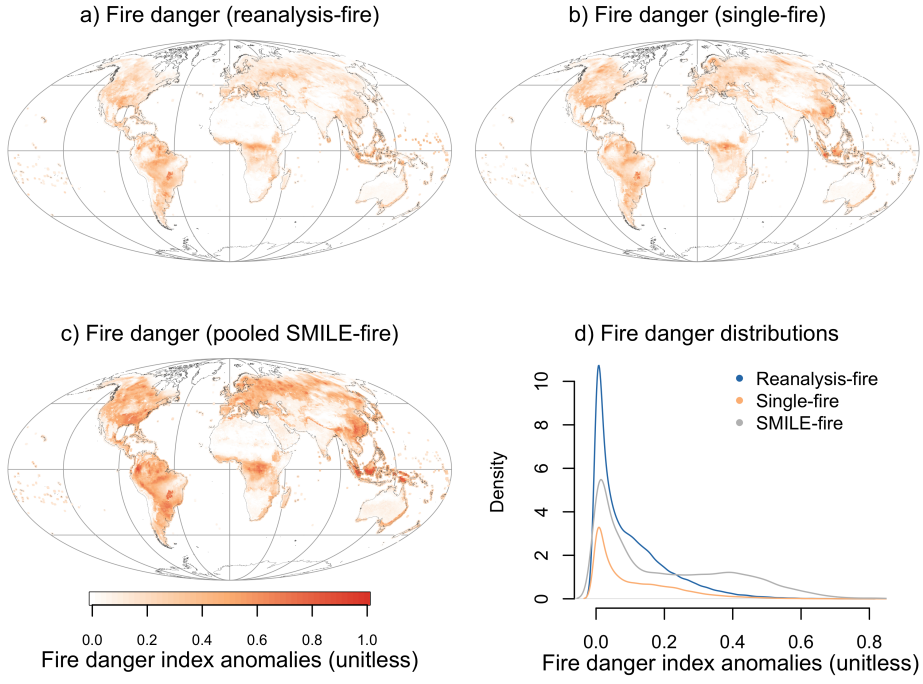

Figure C6. Maximum value of fire danger index (FDI). (a) reanalysis simulation based on the reanalysis forcing. (b) single-member run (r1i1p1f1). (c) Pooled large ensemble (r1i1p1f1 to r40i1p1f1).

References

Andela, N., Morton, D. C., Giglio, L., Chen, Y., Van Der Werf, G. R., Kasibhatla, P. S., DeFries, R. S., Collatz, G. J., Hantson, S., Kloster, S., Bachelet, D., Forrest, M., Lasslop, G., Li, F., Mangeon, S., Melton, J. R., Yue, C., and Randerson, J. T.: A human-driven decline in global burned area, Science, 356, 1356–1362, https://doi.org/10.1126/science.aal4108, 2017.

Bevacqua, E., Michele, C. D., Manning, C., Couasnon, A., Ribeiro, A. F. S., Ramos, A. M., Vignotto, E., Bastos, A., Blesić, S., Durante, F., Hillier, J., Oliveira, S. C., Pinto, J. G., Ragno, E., Rivoire, P., Saunders, K., van der Wiel, K., Wu, W., Zhang, T., and Zscheischler, J.: Guidelines for Studying Diverse Types of Compound Weather and Climate Events, Earth ' s Future, 9, 1–23, https://doi.org/10.1029/2021EF002340, 2021.

Bevacqua, E., Suarez-Gutierrez, L., Jézéquel, A., Lehner, F., Vrac, M., Yiou, P., and Zscheischler, J.: Advancing research on compound weather and climate events via large ensemble model simulations, Nature Communications, 14, 2145, https://doi.org/10.1038/s41467-023-37847-5, 2023.

Bevacqua, E., Fischer, E., Sillmann, J., and Zscheischler, J.: Moderate global warming does not rule out extreme global climate outcomes, Nature, 651, 946–953, 2026.

Cannon, A. J.: Multivariate quantile mapping bias correction: an N-dimensional probability density function transform for climate model simulations of multiple variables, Climate Dynamics, 50, 31–49, https://doi.org/10.1007/s00382-017-3580-6, 2018.

https://doi.org/10.5194/egusphere-2026-2952
Preprint. Discussion started: 5 June 2026

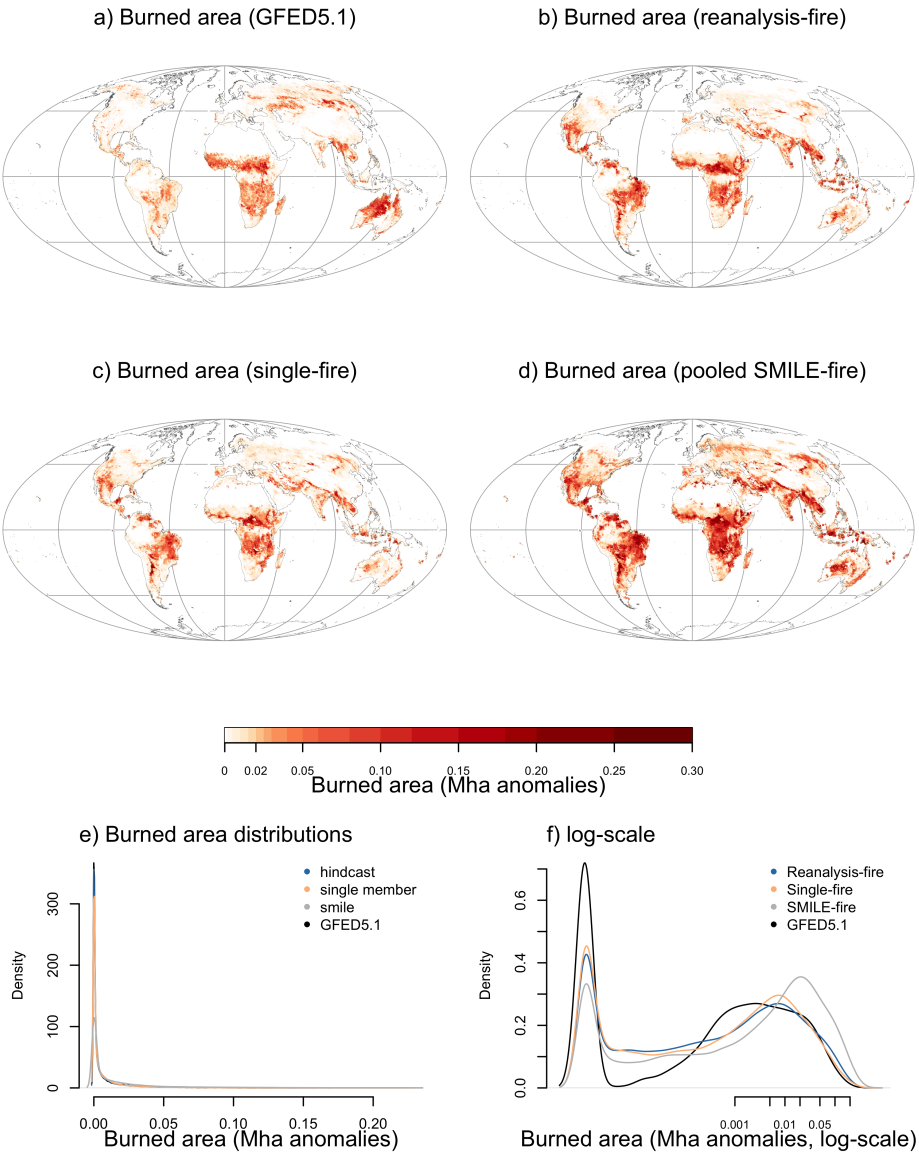

Figure C7. Maximum value of annual sums of burned area. (a) GFEDv5.1 2002-2014 (b) reanalysis simulation based on the reanalysis forcing 1979-2014. (c) single-member run (r1i1p1f1) 1979-2014. (d) Pooled large ensemble (r1i1p1f1 to r40i1p1f1).

https://doi.org/10.5194/egusphere-2026-2952
Preprint. Discussion started: 5 June 2026

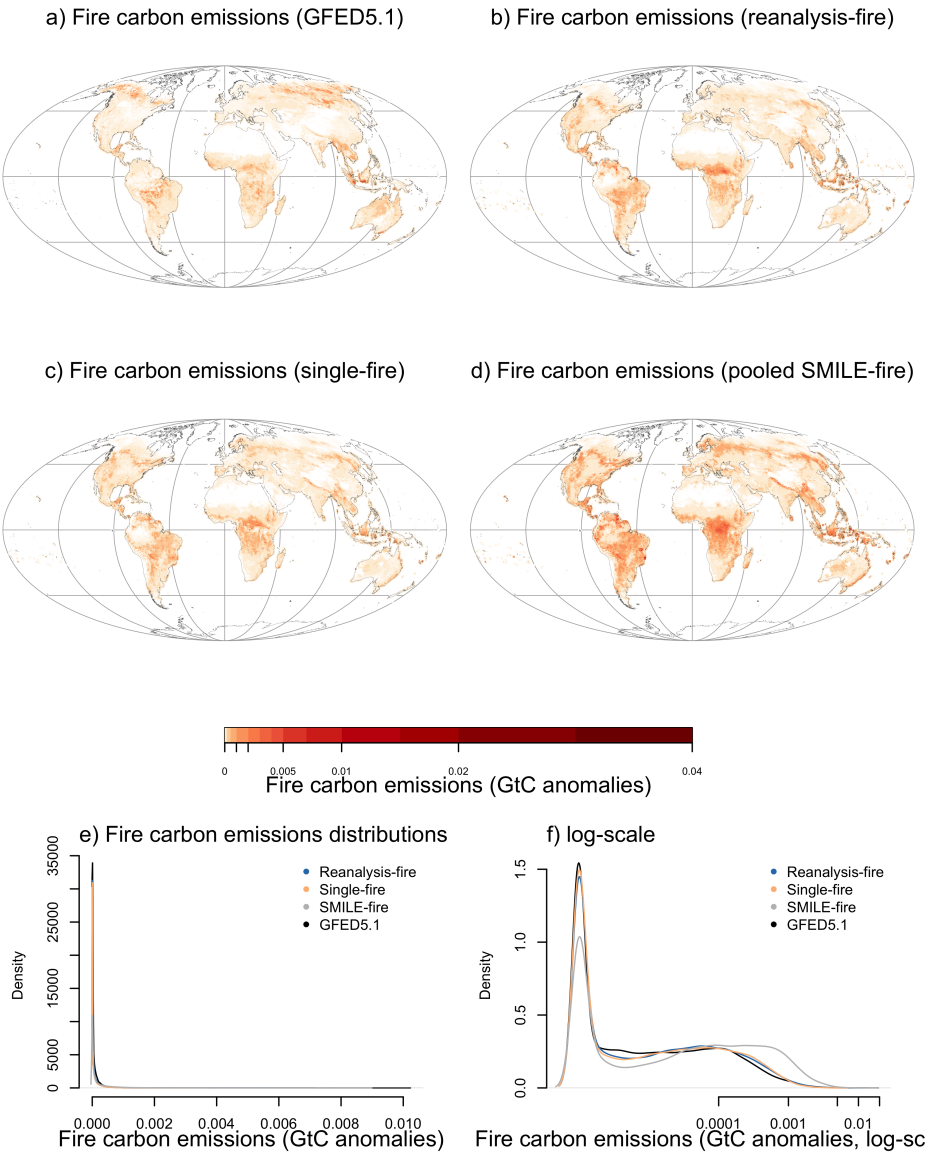

Figure C8. Maximum value of annual sums of fire carbon emissions. (a) GFEDv5.1 2002-2014 (b) reanalysis simulation based on the reanalysis forcing 1979-2014. (c) single-member run (r1i1p1f1) 1979-2014. (d) Pooled large ensemble (r1i1p1f1 to r40i1p1f1).

https://doi.org/10.5194/egusphere-2026-2952
Preprint. Discussion started: 5 June 2026

Chen, Y., Hall, J., Van Wees, D., Andela, N., Hantson, S., Giglio, L., Van Der Werf, G. R., Morton, D. C., and Randerson, J. T.: Multi-decadal trends and variability in burned area from the fifth version of the Global Fire Emissions Database (GFED5), Earth System Science Data, 15, 5227–5259, https://doi.org/10.5194/essd-15-5227-2023, 2023.

Christian, H. J., Blakeslee, R. J., Boccippio, D. J., Boeck, W. L., Buechler, D. E., Driscoll, K. T., Goodman, S. J., Hall, J. M., Koshak, W. J., Mach, D. M., and Stewart, M. F.: Global frequency and distribution of lightning as observed from space by the Optical Transient Detector, Journal of Geophysical Research: Atmospheres, 108, https://doi.org/10.1029/2002jd002347, 2003.

Cucchi, M., Weedon, G. P., Amici, A., Bellouin, N., Lange, S., Müller Schmied, H., Hersbach, H., and Buontempo, C.: WFDE5: bias-adjusted ERA5 reanalysis data for impact studies, Earth System Science Data, 12, 2097–2120, https://doi.org/10.5194/essd-12-2097-2020, 2020.

Cunningham, C. X., Abatzoglou, J. T., Kolden, C. A., Williamson, G. J., Steuer, M., and Bowman, D. M.: Climate-linked escalation of societally disastrous wildfires, Science, 390, 53–58, https://doi.org/10.1126/science.adr5127, 2025.

Deser, C., Phillips, A., Bourdette, V., and Teng, H.: Uncertainty in climate change projections: the role of internal variability, Clim. Dyn., 38, 527–546, 2012.

Dirmeyer, P. A., Gao, X., Zhao, M., Guo, Z., Oki, T., and Hanasaki, N.: GSWP-2: Multimodel Analysis and Implications for Our Perception of the Land Surface, Bulletin of the American Meteorological Society, 87, 1381–1398, https://doi.org/10.1175/BAMS-87-10-1381, 2006.

Drüke, M., Forke, M., Bloh, W. V., Sakschewski, B., Cardoso, M., Bustamante, M., Kurths, J., and Thonicke, K.: Improving the LPJmL4-SPITFIRE vegetation-fire model for South America using satellite data, Geoscientific Model Development, 12, 5029–5054, https://doi.org/10.5194/gmd-12-5029-2019, 2019.

Fader, M., Rost, S., Müller, C., Bondeau, A., and Gerten, D.: Virtual water content of temperate cereals and maize: Present and potential future patterns, Journal of Hydrology, 384, 218–231, https://doi.org/10.1016/j.jhydrol.2009.12.011, 2010.

Feng, S., Zscheischler, J., Hao, Z., and Bevacqua, E.: Growing human-induced climate change fingerprint in regional weekly fire extremes, npj Climate and Atmospheric Science, 8, 1–11, https://doi.org/10.1038/s41612-025-01021-z, 2025.

Forkel, M., Andela, N., P Harrison, S., Lasslop, G., Van Marle, M., Chuvieco, E., Dorigo, W., Forrest, M., Hantson, S., Heil, A., Li, F., Melton, J., Sitch, S., Yue, C., and Arneth, A.: Emergent relationships with respect to burned area in global satellite observations and fire-enabled vegetation models, Biogeosciences, 16, 57–76, https://doi.org/10.5194/bg-16-57-2019, 2019.

Forrest, M., Hetzer, J., Billing, M., Bowring, S. P., Kosczor, E., Oberhagemann, L., Perkins, O., Warren, D., Arrogante-Funes, F., Thonicke, K., and Hickler, T.: Understanding and simulating cropland and non-cropland burning in Europe using the BASE (Burnt Area Simulator for Europe) model, Biogeosciences, 21, 5539–5560, https://doi.org/10.5194/bg-21-5539-2024, 2024.

Giglio, L., van der Werf, G. R., Randerson, J. T., Collatz, G. J., and Kasibhatla, P.: Global estimation of burned area using MODIS active fire observations, Atmospheric Chemistry and Physics, 6, 957–974, https://doi.org/10.5194/acp-6-957-2006, 2006.

Hantson, S., Kelley, D. I., Arneth, A., Harrison, S. P., Archibald, S., Bachelet, D., Forrest, M., Hickler, T., Lasslop, G., Li, F., Mangeon, S., Melton, J. R., Nieradzik, L., Rabin, S. S., Colin Prentice, I., Sheehan, T., Sitch, S., Teckentrup, L., Voulgarakis, A., and Yue, C.: Quantitative assessment of fire and vegetation properties in simulations with fire-enabled vegetation models from the Fire Model Intercomparison Project, Geoscientific Model Development, 13, 3299–3318, https://doi.org/10.5194/gmd-13-3299-2020, 2020.

Hantson, S., Hamilton, D. S., and Burton, C.: Changing fire regimes: Ecosystem impacts in a shifting climate, One Earth, 7, 942–945, https://doi.org/10.1016/j.oneear.2024.05.021, 2024.

Jain, S., Scaife, A. A., Shepherd, T. G., Deser, C., Dunstone, N., Schmidt, G. A., Trenberth, K. E., and Turkington, T.: Importance of internal variability for climate model assessment, Npj Clim. Atmos. Sci., 6, 2023.

https://doi.org/10.5194/egusphere-2026-2952
Preprint. Discussion started: 5 June 2026

Janssen, T. A., Jones, M. W., Finney, D., van der Werf, G. R., van Wees, D., Xu, W., and Veraverbeke, S.: Extratropical forests increasingly at risk due to lightning fires, Nature Geoscience, 16, 1136–1144, https://doi.org/10.1038/s41561-023-01322-z, 2023.

Jones, M. W., Abatzoglou, J. T., Veraverbeke, S., Andela, N., Lasslop, G., Forkel, M., Smith, A. J. P., Burton, C., Betts, R. A., van der Werf, G. R., Sitch, S., Canadell, J. G., Santín, C., Kolden, C., Doerr, S. H., and Le Quéré, C.: Global and Regional Trends and Drivers of Fire Under Climate Change, Reviews of Geophysics, 60, e2020RG000 726, https://doi.org/https://doi.org/10.1029/2020RG000726, 2022.

Jones, M. W., Kelley, D. I., Burton, C. A., Di Giuseppe, F., Barbosa, M. L. F., Brambleby, E., Hartley, A. J., Lombardi, A., Mataveli, G., McNorton, J. R., Spuler, F. R., Wessel, J. B., Abatzoglou, J. T., Anderson, L. O., Andela, N., Archibald, S., Armenteras, D., Burke, E., Carmenta, R., Chuvieco, E., Clarke, H., Doerr, S. H., Fernandes, P. M., Giglio, L., Hamilton, D. S., Hantson, S., Harris, S., Jain, P., Kolden, C. A., Kurvits, T., Lampe, S., Meier, S., New, S., Parrington, M., Perron, M. M. G., Qu, Y., Ribeiro, N. S., Saharjo, B. H., San-Miguel-Ayanz, J., Shuman, J. K., Tanpipat, V., van der Werf, G. R., Veraverbeke, S., and Xanthopoulos, G.: State of Wildfires 2023–2024, Earth System Science Data, 16, 3601–3685, https://doi.org/10.5194/essd-16-3601-2024, 2024.

Keeping, T. R., Zhou, B., Cai, W., Shepherd, T. G., Prentice, I. C., van der Wiel, K., and Harrison, S. P.: Present and future interannual variability in wildfire occurrence: a large ensemble application to the United States, Frontiers in Forests and Global Change, 8, 1–12, https://doi.org/10.3389/ffgc.2025.1519836, 2025.

Kelder, T., Wanders, N., Van Der Wiel, K., Marjoribanks, T. I., Slater, L. J., Wilby, R. L., and Prudhomme, C.: Interpreting extreme climate impacts from large ensemble simulations - Are they unseen or unrealistic?, Environmental Research Letters, 17, https://doi.org/10.1088/1748-9326/ac5cf4, 2022.

Kelder, T., Heinrich, D., Klok, L., Thompson, V., Goulart, H. M. D., Hawkins, E., Slater, L. J., Suarez-Gutierrez, L., Wilby, R. L., Coughlan De Perez, E., Stephens, E. M., Burt, S., Van Den Hurk, B., De Vries, H., Van Der Wiel, K., Schipper, E. L. F., Carmona Baéz, A., Van Bueren, E., and Fischer, E. M.: How to Stop Being Surprised by Unprecedented Weather, Nature Communications, 16, 2382, https://doi.org/10.1038/s41467-025-57450-0, 2025.

Kelley, D. I., Burton, C., Di Giuseppe, F., Jones, M. W., Barbosa, M. L. F., Brambleby, E., McNorton, J. R., Liu, Z., Bradley, A. S. I., Blackford, K., Burke, E., Ciavarella, A., Di Tomaso, E., Eden, J., Ferreira, I. J. M., Fiedler, L., Hartley, A. J., Keeping, T. R., Lampe, S., Lombardi, A., Mataveli, G., Qu, Y., Silva, P. S., Spuler, F. R., Steinmann, C. B., Torres-Vázquez, M. Á., Veiga, R., van Wees, D., Wessel, J. B., Wright, E., Bilbao, B., Bourbonnais, M., Gao, C., Di Bella, C. M., Dintwe, K., Donovan, V. M., Harris, S., Kukavskaya, E. A., N'Dri, A. B., Santín, C., Selaya, G., Sjöström, J., Abatzoglou, J. T., Andela, N., Carmenta, R., Chuvieco, E., Giglio, L., Hamilton, D. S., Hantson, S., Meier, S., Parrington, M., Sadegh, M., San-Miguel-Ayanz, J., Sedano, F., Turco, M., van der Werf, G. R., Veraverbeke, S., Anderson, L. O., Clarke, H., Fernandes, P. M., and Kolden, C. A.: State of Wildfires 2024–2025, Earth System Science Data, 17, 5377–5488, https://doi.org/10.5194/essd-17-5377-2025, 2025.

Kim, H.: Global Soil Wetness Project Phase 3 Atmospheric Boundary Conditions (Experiment 1), https://doi.org/10.20783/DIAS.501, 2017.

Klein Goldewijk, K., Beusen, A., Van Drecht, G., and De Vos, M.: The HYDE 3.1 spatially explicit database of human-induced global land-use change over the past 12,000 years, Global Ecology and Biogeography, 20, 73–86, https://doi.org/10.1111/j.1466-8238.2010.00587.x, 2011.

Lange, S.: Trend-preserving bias adjustment and statistical downscaling with ISIMIP3BASD (v1.0), Geoscientific Model Development, 12, 3055–3070, https://doi.org/10.5194/gmd-12-3055-2019, 2019.

Lange, S.: ISIMIP3BASD v2.5.0, https://doi.org/10.5281/zenodo.4686991, 2020.

Lange, S.: ISIMIP3b bias adjustment fact sheet, ISIMIP Repository, p. 39, https://www.isimip.org/documents/413/ISIMIP3b_bias_adjustment_fact_sheet_Gnsz7CO.pdf, 2021.

https://doi.org/10.5194/egusphere-2026-2952
Preprint. Discussion started: 5 June 2026

Lange, S., Menz, C., Gleixner, S., Cucchi, M., Weedon, G. P., Amici, A., Bellouin, N., Müller-Schmied, H., Hersbach, H., Buontempo, C., and Cagnazzo, C.: WFDE5 over land merged with ERA5 over the ocean (W5E5 v2.0), https://doi.org/10.48364/ISIMIP.342217, 2021.

Le Quéré, C., Moriarty, R., Andrew, R. M., Canadell, J. G., Sitch, S., Korsbakken, J. I., Friedlingstein, P., Peters, G. P., Andres, R. J., Boden, T. A., Houghton, R. A., House, J. I., Keeling, R. F., Tans, P., Arneth, A., Bakker, D. C., Barbero, L., Bopp, L., Chang, J., Chevallier, F., Chini, L. P., Ciais, P., Fader, M., Feely, R. A., Gkritzalis, T., Harris, I., Hauck, J., Ilyina, T., Jain, A. K., Kato, E., Kitidis, V., Klein Goldewijk, K., Koven, C., Landschützer, P., Lauvset, S. K., Lefèvre, N., Lenton, A., Lima, I. D., Metzl, N., Millero, F., Munro, D. R., Murata, A., S. Nabel, J. E., Nakaoka, S., Nojiri, Y., O'Brien, K., Olsen, A., Ono, T., Pérez, F. F., Pfeil, B., Pierrot, D., Poulter, B., Rehder, G., Rödenbeck, C., Saito, S., Schuster, U., Schwinger, J., Séférian, R., Steinhoff, T., Stocker, B. D., Sutton, A. J., Takahashi, T., Tilbrook, B., Van Der Laan-Luijkx, I. T., Van Der Werf, G. R., Van Heuven, S., Vandemark, D., Viovy, N., Wiltshire, A., Zaehle, S., and Zeng, N.: Global Carbon Budget 2015, Earth System Science Data, 7, 349–396, https://doi.org/10.5194/essd-7-349-2015, 2015.

Lehner, F.: Climate model large ensembles as test beds for applied compound event research, iScience, 27, 111 113, https://doi.org/https://doi.org/10.1016/j.isci.2024.111113, 2024.

Lehner, F., Deser, C., Maher, N., Marotzke, J., Fischer, E. M., Brunner, L., Knutti, R., and Hawkins, E.: Partitioning climate projection uncertainty with multiple large ensembles and CMIP5/6, Earth Syst. Dyn., 11, 491–508, 2020.

Li, F., Lawrence, D. M., Rogers, B. M., Burton, C., Huang, H., Jiang, Y., Kaiser, J. W., Kasoar, M., Lee, H., Leung, R., Nieradzik, L., and Wang, A.: The Fire Modeling Intercomparison Project (FireMIP) for CMIP7, Geophysical Model Development, pp. 3989–4007, 2026.

Mackallah, C., Chamberlain, M. A., Law, R. M., Dix, M., Ziehn, T., Bi, D., Bodman, R., Brown, J. R., Dobrohotoff, P., Druken, K., Evans, B., Harman, I. N., Hayashida, H., Holmes, R., Kiss, A. E., Lenton, A., Liu, Y., Marsland, S., Meissner, K., Menviel, L., O'farrell, S., Rashid, H. A., Ridzwan, S., Savita, A., Srbinovsky, J., Sullivan, A., Trenham, C., Vohralik, P. F., Wang, Y. P., Williams, G., Woodhouse, M. T., and Yeung, N.: ACCESS datasets for CMIP6: Methodology and idealised experiments, Journal of Southern Hemisphere Earth Systems Science, 72, 93–116, https://doi.org/10.1071/ES21031, 2022.

Meyn, A., Taylor, S. W., Flannigan, M. D., Thonicke, K., and Cramer, W.: Relationship between fire, climate oscillations, and drought in British Columbia, Canada, 1920-2000, Global Change Biology, 16, 977–989, https://doi.org/10.1111/j.1365-2486.2009.02061.x, 2010.

Oberhagemann, L., Billing, M., von Bloh, W., Drüke, M., Forrest, M., Bowring, S. P. K., Hetzer, J., Ribalaygua Batalla, J., and Thonicke, K.: Sources of uncertainty in the SPITFIRE global fire model: development of LPJmL-SPITFIRE1.9 and directions for future improvements, Geoscientific Model Development, 18, 2021–2050, https://doi.org/10.5194/gmd-18-2021-2025, 2025.

Quilcaille, Y., Batibeniz, F., Ribeiro, A. F. S., Padrón, R. S., and Seneviratne, S. I.: Fire weather index data under historical and shared socioeconomic pathway projections in the 6th phase of the Coupled Model Intercomparison Project from 1850 to 2100, Earth System Science Data, 15, 2153–2177, https://doi.org/10.5194/essd-15-2153-2023, 2023.

Ribeiro, A. F. S., Brando, P. M., Santos, L., Rattis, L., Hirschi, M., Hauser, M., Seneviratne, S. I., and Zscheischler, J.: A compound event-oriented framework to tropical fire risk assessment in a changing climate, Environmental Research Letters, https://doi.org/https://doi.org/10.1088/1748-9326/ac7342, 2022.

Ribeiro, A. F. S., Santos, L., Randerson, J. T., Uribe, M. R., Alencar, A. A. C., Macedo, M. N., Morton, D. C., Zscheischler, J., Silvestrini, R. A., Rattis, L., Seneviratne, S. I., and Brando, P. M.: The time since land-use transition drives changes in fire activity in the Amazon-Cerrado region, Communications Earth & Environment, 5, 96, https://doi.org/10.1038/s43247-024-01248-3, 2024.

Richardson, D., Ribeiro, A. F., Batibeniz, F., Quilcaille, Y., Taschetto, A. S., Pitman, A. J., and Zscheischler, J.: Increasing Fire Weather Season Overlap Between North America and Australia Challenges Firefighting Cooperation, Earth's Future, 13, https://doi.org/10.1029/2024EF005030, 2025.

https://doi.org/10.5194/egusphere-2026-2952
Preprint. Discussion started: 5 June 2026

Schaphoff, S., von Bloh, W., Rammig, A., Thonicke, K., Biemans, H., Forkel, M., Gerten, D., Heinke, J., Jägermeyr, J., Knauer, J., Langerwisch, F., Lucht, W., Müller, C., Rolinski, S., and Waha, K.: LPJmL4 – a dynamic global vegetation model with managed land – Part 1: Model description, Geoscientific Model Development, 11, 1343–1375, https://doi.org/10.5194/gmd-11-1343-2018, 2018.

Shepherd, T. G., Boyd, E., Calel, R. A., Chapman, S. C., Dessai, S., Dima-West, I. M., Fowler, H. J., James, R., Maraun, D., Martius, O., Senior, C. A., Sobel, A. H., Stainforth, D. A., Tett, S. F., Trenberth, K. E., van den Hurk, B. J., Watkins, N. W., Wilby, R. L., and Zenghelis, D. A.: Storylines: an alternative approach to representing uncertainty in physical aspects of climate change, Climatic Change, 151, 555–571, https://doi.org/10.1007/s10584-018-2317-9, 2018.

Sillmann, J., Shepherd, T. G., van den Hurk, B., Hazeleger, W., Martius, O., Slingo, J., and Zscheischler, J.: Event-Based Storylines to Address Climate Risk, https://doi.org/10.1029/2020EF001783, 2021.

Spuler, F. R., Wessel, J. B., Comyn-Platt, E., Varndell, J., and Cagnazzo, C.: ibicus: a new open-source Python package and comprehensive interface for statistical bias adjustment and evaluation in climate modelling (v1.0.1), Geosci. Model Dev., 17, 1249–1269, 2024.

Spuler, F. R., Wessel, J. B., Jebeile, J., Zscheischler, J., and Shepherd, T. G.: Bias Adjustment and the Question of Usable Climate Information: Methodological Assumptions and Value Judgments, Bulletin of the American Meteorological Society, 107, https://doi.org/10.1175/BAMS-D-25-0022.1, 2026.

Switanek, M. B., Troch, P. A., Castro, C. L., Leuprecht, A., Chang, H.-I., Mukherjee, R., and Demaria, E. M. C.: Scaled distribution mapping: a bias correction method that preserves raw climate model projected changes, Hydrol. Earth Syst. Sci., 21, 2649–2666, 2017.

Teckentrup, L., Harrison, S. P., Hantson, S., Heil, A., Melton, J. R., Forrest, M., Li, F., Yue, C., Arneth, A., Hickler, T., Sitch, S., and Lasslop, G.: Response of simulated burned area to historical changes in environmental and anthropogenic factors: a comparison of seven fire models, Biogeosciences, 16, 3883–3910, https://doi.org/10.5194/bg-16-3883-2019, 2019.

Thonicke, K., Spessa, A., Prentice, I. C., Harrison, S. P., Dong, L., and Carmona-Moreno, C.: The influence of vegetation, fire spread and fire behaviour on biomass burning and trace gas emissions: Results from a process-based model, Biogeosciences, 7, 1991–2011, https://doi.org/10.5194/bg-7-1991-2010, 2010.

Touma, D., Stevenson, S., Lehner, F., and Coats, S.: Human-driven greenhouse gas and aerosol emissions cause distinct regional impacts on extreme fire weather, Nature Communications, 12, 1–8, https://doi.org/10.1038/s41467-020-20570-w, 2021.

Tschumi, E., Lienert, S., van der Wiel, K., Joos, F., and Zscheischler, J.: The effects of varying drought-heat signatures on terrestrial carbon dynamics and vegetation composition, Biogeosciences, 19, 1979–1993, https://doi.org/10.5194/bg-19-1979-2022, 2022.

Tschumi, E., Lienert, S., Bastos, A., Ciais, P., Gregor, K., Joos, F., Knauer, J., Papastefanou, P., Rammig, A., van der Wiel, K., Williams, K., Xu, Y., Zaehle, S., and Zscheischler, J.: Large Variability in Simulated Response of Vegetation Composition and Carbon Dynamics to Variations in Drought-Heat Occurrence, Journal of Geophysical Research: Biogeosciences, 128, e2022JG007 332, https://doi.org/https://doi.org/10.1029/2022JG007332, 2023.

Undorf, S.: ISIMIP3BASD-LE, https://doi.org/10.5281/zenodo.10377116, 2023.

Van Der Werf, G. R., Randerson, J. T., Giglio, L., Van Leeuwen, T. T., Chen, Y., Rogers, B. M., Mu, M., Van Marle, M. J., Morton, D. C., Collatz, G. J., Yokelson, R. J., and Kasibhatla, P. S.: Global fire emissions estimates during 1997-2016, Earth System Science Data, 9, 697–720, https://doi.org/10.5194/essd-9-697-2017, 2017.

van der Werf, G. R., Randerson, J. T., van Wees, D., Chen, Y., Giglio, L., Hall, J., Roland, V., Mu, M., Binte Shahid, S., Barsanti, K. C., Yokelson, R., and Morton, D. C.: Landscape fire emissions from the 5th version of the Global Fire Emissions Database (GFED5), Scientific Data, 12, 1–18, https://doi.org/10.1038/s41597-025-06127-w, 2025.

https://doi.org/10.5194/egusphere-2026-2952
Preprint. Discussion started: 5 June 2026

van der Wiel, K., Selten, F. M., Bintanja, R., Blackport, R., and Screen, J. A.: Added value of large ensemble simulations for assessing extreme river discharge in a 2 °C warmer world, Geophysical Research Letters, 46, 2093–2102, https://doi.org/10.1029/2019GL081967, 2019.

Van Der Wiel, K., Selten, F. M., Bintanja, R., Blackport, R., and Screen, J. A.: Ensemble climate-impact modelling: extreme impacts from moderate meteorological conditions, Environmental Research Letters, 15, https://doi.org/10.1088/1748-9326/ab7668, 2020.

Vogel, J., Rivoire, P., Deidda, C., Rahimi, L., Sauter, C. A., Tschumi, E., van der Wiel, K., Zhang, T., and Zscheischler, J.: Identifying meteorological drivers of extreme impacts: an application to simulated crop yields, Earth System Dynamics, 12, 151–172, https://doi.org/10.5194/esd-12-151-2021, 2021.

Von Bloh, W., Schaphoff, S., Müller, C., Rolinski, S., Waha, K., and Zaehle, S.: Implementing the nitrogen cycle into the dynamic global vegetation, hydrology, and crop growth model LPJmL (version 5.0), Geoscientific Model Development, 11, 2789–2812, https://doi.org/10.5194/gmd-11-2789-2018, 2018.

Wagner, C. V.: Development and structure of the Canadian forest fire weather index system., 35, 1987.

Ward, D. S., Shevliakova, E., Malyshev, S., and Rabin, S.: Trends and Variability of Global Fire Emissions Due To Historical Anthropogenic Activities, Global Biogeochemical Cycles, 32, 122–142, https://doi.org/10.1002/2017GB005787, 2018.

Warszawski, L., Frieler, K., Huber, V., Piontek, F., Serdeczny, O., and Schewe, J.: The inter-sectoral impact model intercomparison project (ISI-MIP): Project framework, Proceedings of the National Academy of Sciences of the United States of America, 111, 3228–3232, https://doi.org/10.1073/pnas.1312330110, 2014.

Wirth, S. B., Braun, J., Heinke, J., Ostberg, S., Rolinski, S., Schaphoff, S., Stenzel, F., von Bloh, W., Taube, F., and Müller, C.: Biological nitrogen fixation of natural and agricultural vegetation simulated with LPJmL 5.7.9, Geosci. Model Dev., 17, 889–7914, https://doi.org/10.5194/gmd-17-7889-2024, 2024.

Zscheischler, J., Michalak, A. M., Schwalm, C., Mahecha, M. D., Huntzinger, D. N., Reichstein, M., Berthier, G., Ciais, P., Cook, R. B., El-Masri, B., Huang, M., Ito, A., Jain, A., King, A., Lei, H., Lu, C., Mao, J., Peng, S., Poulter, B., Ricciuto, D., Shi, X., Tao, B., Tian, H., Viovy, N., Wang, W., Wei, Y., Yang, J., and Zeng, N.: Impact of large-scale climate extremes on biospheric carbon fluxes: An intercomparison based on MsTMIP data, Global Biogeochemical Cycles, 28, 585–600, https://doi.org/10.1002/2014GB004826, 2014.

Zscheischler, J., Martius, O., Westra, S., Bevacqua, E., Raymond, C., Horton, R. M., van den Hurk, B., AghaKouchak, A., Jézéquel, A., Mahecha, M. D., Maraun, D., Ramos, A. M., Ridder, N. N., Thiery, W., and Vignotto, E.: A Typology of Compound Weather and Climate Events, Nature Reviews Earth & Environment, 1, 333–347, https://doi.org/10.1038/s43017-020-0060-z, 2020.